Preliminary Aerodynamic Investigation of Fan Rotor Blade Morphing

Daniel L. Tweedt
AP Solutions, Inc., Cleveland, Ohio

NASA STI Program . . . in Profile

Since its founding, NASA has been dedicated to the advancement of aeronautics and space science. The NASA Scientific and Technical Information (STI) program plays a key part in helping NASA maintain this important role.

The NASA STI Program operates under the auspices of the Agency Chief Information Officer. It collects, organizes, provides for archiving, and disseminates NASA's STI. The NASA STI program provides access to the NASA Aeronautics and Space Database and its public interface, the NASA Technical Reports Server, thus providing one of the largest collections of aeronautical and space science STI in the world. Results are published in both non-NASA channels and by NASA in the NASA STI Report Series, which includes the following report types:

- TECHNICAL PUBLICATION. Reports of completed research or a major significant phase of research that present the results of NASA programs and include extensive data or theoretical analysis. Includes compilations of significant scientific and technical data and information deemed to be of continuing reference value. NASA counterpart of peer-reviewed formal professional papers but has less stringent limitations on manuscript length and extent of graphic presentations.

- TECHNICAL MEMORANDUM. Scientific and technical findings that are preliminary or of specialized interest, e.g., quick release reports, working papers, and bibliographies that contain minimal annotation. Does not contain extensive analysis.

- CONTRACTOR REPORT. Scientific and technical findings by NASA-sponsored contractors and grantees.

- CONFERENCE PUBLICATION. Collected papers from scientific and technical conferences, symposia, seminars, or other meetings sponsored or cosponsored by NASA.

- SPECIAL PUBLICATION. Scientific, technical, or historical information from NASA programs, projects, and missions, often concerned with subjects having substantial public interest.

- TECHNICAL TRANSLATION. English-language translations of foreign scientific and technical material pertinent to NASA's mission.

Specialized services also include creating custom thesauri, building customized databases, organizing and publishing research results.

For more information about the NASA STI program, see the following:

- Access the NASA STI program home page at *http://www.sti.nasa.gov*

- E-mail your question to *help@sti.nasa.gov*

- Fax your question to the NASA STI Information Desk at 443–757–5803

- Phone the NASA STI Information Desk at 443–757–5802

- Write to:
  STI Information Desk
  NASA Center for AeroSpace Information
  7115 Standard Drive
  Hanover, MD 21076–1320

NASA/CR—2012-217815

Preliminary Aerodynamic Investigation of Fan Rotor Blade Morphing

Daniel L. Tweedt
AP Solutions, Inc., Cleveland, Ohio

National Aeronautics and
Space Administration

Glenn Research Center
Cleveland, Ohio 44135

December 2012

Level of Review: This material has been technically reviewed by NASA technical management OR expert reviewer(s).

Preliminary Aerodynamic Investigation of Fan Rotor Blade Morphing

Daniel L. Tweedt
AP Solutions, Inc.
Cleveland, Ohio 44135

Abstract

Various new technologies currently under development may enable controlled blade shape variability, or so-called blade morphing, to be practically employed in aircraft engine fans and compressors in the foreseeable future. The current study is a relatively brief, preliminary computational fluid dynamics investigation aimed at partially demonstrating and quantifying the aerodynamic potential of fan rotor blade morphing. The investigation is intended to provide information useful for near-term planning, as well as aerodynamic solution data sets that can be subsequently analyzed using advanced acoustic diagnostic tools, for the purpose of making fan noise comparisons.

Two existing fan system models serve as baselines for the investigation: the Advanced Ducted Propulsor fan with a design tip speed of 806 ft/sec and a pressure ratio of 1.294, and the Source Diagnostic Test fan with a design tip speed of 1215 ft/sec and a pressure ratio of 1.470. Both are 22-inch sub-scale, low-noise research fan/nacelle models that have undergone extensive experimental testing in the 9- by 15-foot Low Speed Wind Tunnel at the NASA Glenn Research Center.

The study, restricted to fan rotor blade morphing only, involves a fairly simple blade morphing technique. Specifically, spanwise-linear variations in rotor blade-section setting angle are applied to alter the blade shape; that is, the blade is linearly retwisted from hub to tip. Aerodynamic performance comparisons are made between morphed-blade and corresponding baseline configurations on the basis of equal fan system thrust, where rotor rotational speed for the morphed-blade fan is varied to change the thrust level for that configuration.

The results of the investigation confirm that rotor blade morphing could be a useful technology, with the potential to enable significant improvements in fan aerodynamic performance. Even though the study is very limited in scope and confined to simple geometric perturbations of two existing fan systems, the aerodynamic effectiveness of blade morphing is demonstrated by the configurations analyzed. In particular, for the Advanced Ducted Propulsor fan it is demonstrated that the performance levels of the original variable-pitch baseline design can be achieved using blade morphing instead of variable pitch, and for the Source Diagnostic Test fan the performance at important off-design operating points is substantially increased with blade morphing.

Introduction

Various new technologies currently under development may enable controlled blade shape variability, or so-called blade morphing, to be practically employed in aircraft engine fans and compressors in the foreseeable future. Information regarding the potential aerodynamic benefits of blade morphing would be useful for ongoing advocacy, prioritizing, and planning of near-term research in this area.

The current study is a relatively brief, preliminary computational fluid dynamics (CFD) investigation aimed at partially demonstrating and quantifying the aerodynamic potential of fan rotor blade morphing. The investigation is intended to provide information useful for near-term planning, as well as CFD solution data sets that can be subsequently analyzed using advanced acoustic diagnostic tools, if desired, for the purpose of making fan noise comparisons.

Two existing fan system models serve as baselines for the investigation. The first system, the Advanced Ducted Propulsor (ADP) fan, version 1, was designed by United Technologies Corporation, Pratt & Whitney [1,2][†] with NASA funding under the Advanced Subsonic Technology program. The ADP fan is a 22-inch sub-scale, low-noise research fan/nacelle model that has undergone extensive experimental testing in the 9- by 15-foot Low Speed Wind Tunnel (LSWT) at the NASA Glenn Research Center [3]. The second system, the Source Diagnostic Test (SDT) fan, was designed by the General Electric Corporation with partial funding from NASA under the Advanced Subsonic Technology program. The SDT fan is also a 22-inch sub-scale, low-noise research fan/nacelle model that has undergone extensive experimental testing in the LSWT [4,5].

Due to limited time and resource constraints, the present study is restricted to fan rotor blade morphing only, and a fairly simple blade morphing technique is used. Specifically, spanwise-linear variations in rotor blade-section setting angle are applied to alter the blade shape; that is, the blade is linearly retwisted from hub to tip. The amount of morphing is quantified by the "tip morph angle", which is the change in blade tip-section setting angle relative to the hub-section setting angle.

Aerodynamic performance comparisons between morphed-blade and corresponding baseline configurations are made on the basis of equal fan system thrust, where rotor rotational speed for the morphed-blade fan is varied to change the thrust level for that configuration. Linear interpolation or extrapolation of the computed solutions is used to exactly match the baseline thrust.

Three simulated flight conditions are included in the investigation. They are takeoff, cruise, and approach, where the approach condition is considered here only for the SDT fan system. Computationally, flight conditions are set by far-field boundary values, especially Mach number and the related static-to-total pressure ratio. Takeoff and approach far-field conditions are the same and correspond to standard-day sea-level (SSL) flight at Mach number 0.100. Cruise conditions correspond to standard-day flight at 30,000 feet and Mach number 0.800 for the ADP fan system, or Mach number 0.780 for the SDT fan system.

---

† Numbers in square brackets indicate references.

Fan System Models

Both fan system models employed for the CFD investigation are fairly complete, including all major fan system components such as engine inlet, fan rotor, fan exit guide vane (FEGV) row, fan nozzle, and engine nacelle. Of the two systems, the SDT model is simpler because it involves only a single flow path along with a fixed-pitch rotor, while the ADP model involves a flow path split (into core and bypass streams) between the rotor and FEGV row, and the rotor is variable pitch. Both systems are described in more detail below, along with the rotor morphed-blade configurations investigated for each.

ADP Fan System

A meridional-plane drawing of the ADP fan system is shown in Figure 1, where all major components are depicted and shown to scale. The rotor blade stacking line is the zero-reference axial location, and the number of blades for each blade row is indicated in parenthesis. It should be noted that downstream of the core inlet guide vane (CIGV) row, the fan system hardware involves a long core-duct (not shown) that extends downstream to well beyond the fan nozzle exit. This core duct is not included in the CFD model.

Because the ADP rotor is a variable-pitch rotor, there are essentially two reference, or baseline, blade shapes for it, one for cruise and one for takeoff. The geometry of the blade itself is the same at both conditions, but the variable-pitch blade setting angle is different by 9.0 degrees. At cruise, which is the aerodynamic design point, the blades are staggered to be more open; that is, they are set to be more aligned with the axial direction. For takeoff the variable-pitch blades are restaggered by rotation about the rotor stacking axis to a more closed setting angle. Corrected[†] rotational speed also differs for the two operating points: at takeoff the speed is 8750 rpm (100 percent), and at cruise the speed is 8397 rpm (96.0 percent)[‡]. The corresponding linear tip speeds for takeoff and cruise are 840 and 806 ft/sec, respectively. A uniform rotor tip clearance of 0.020 inches was used for all CFD simulations at both speeds.

Two different blade morphing schedules, or schemes, were applied to the ADP fan rotor, with the intent to determine if morphing could be an acceptable substitute for rotor blade reset. It was anticipated that this might demonstrate, quantitatively, the potential aerodynamic effectiveness of blade morphing, and possibly also show a practical use for it, assuming that the hardware mechanisms needed to achieve morphing are substantially lighter and less complex than those associated with variable pitch (blade reset).

The first morphing scheme involves an intermediate hub-section setting angle that is midway between the baseline takeoff and baseline cruise setting angles, that is, a -4.5 degree hub reset relative to the takeoff position[§], with blade tip morph angles of +5.0 and -7.0 degrees at

---

† The term "corrected" as applied to rotational speed, mass flow rate, or thrust is terse for "corrected to standard-day sea-level conditions".

‡ For this investigation the corrected rotational speed at takeoff is used as the reference speed, even though the fan design point is at cruise.

§ Negative setting-angle changes, including blade tip morph values, correspond to decreased blade section setting angles, where the blade chord is oriented more in the axial direction and the blade passages are more open.

takeoff and cruise, respectively. Initially, a tip morph angle of -5.0 degrees was selected for cruise, but using an angle of -7.0 degrees provides a significant improvement in aerodynamic performance.

The second schedule involves the takeoff hub-section setting angle, corresponding to a 0.0 degree reset, with blade tip morph angles of 0.0 and -10.0 degrees at takeoff and cruise, respectively. Note that since the blade is not morphed at takeoff, the fan operating point there is the same as the baseline.

SDT Fan System

A meridional-plane drawing of the SDT fan system is shown in Figure 2. As in the previous figure, all major components are depicted and shown to scale, the rotor blade stacking line is the zero-reference axial location, and the number of blades for each blade row is indicated in parenthesis. Like for the ADP fan, the SDT aerodynamic design point is at the cruise operating condition. The SDT rotor blades, however, are fixed at the hub, which is vastly more conventional, and the corrected rotational speed of 12,657 rpm (100 percent) for cruise is also used at takeoff. The corresponding linear tip speed is 1,215 ft/sec. A uniform rotor tip clearance of 0.034 inches was used for all CFD simulations at takeoff and cruise, while a clearance of 0.043 inches was used for approach.

Only a single blade morphing schedule was applied to the SDT fan rotor, with the objective of improving fan performance. Note that this goal is very different from the one mentioned above for the ADP fan. Since the SDT fan aerodynamic design point corresponds to cruise operation, the blade geometry there was taken as the reference shape, and morphing was applied only at the takeoff and approach operating conditions, where for both a tip morph angle of -5.0 degrees was investigated. At approach, with a baseline fan rotational speed of 7,809 rpm (61.7 percent), a second tip morph angle of -10.0 degrees was also investigated. Note that with regard to fan performance at either of these operating conditions, it should be recognized that there are multiple figures of merit; for example, adiabatic efficiency, stall margin, transient response, and noise.

Computational Fluid Dynamics

Flow field simulations were done using two different CFD codes: an axisymmetric viscous solver called AVCS, and a three-dimensional viscous turbomachinery solver called TSWIFT. Multiple solution domains (grid blocks) were used, with axisymmetric solutions coupled to three-dimensional solutions at mixing planes by means of a separate computer program called SMPI, developed as a companion program for AVCS and TSWIFT. SMPI was also used to couple rotating and stationary three-dimensional solutions together at mixing planes. In general, the three-dimensional TSWIFT solver was used for computational domains in and near blade rows, and the axisymmetric AVCS solver was used for computational domains sufficiently far away from blade rows; that is, far enough away that pitchwise (or circumferential) variations can be ignored. All program-to-program data exchange, for mixing planes and direct block-to-block interfaces, was performed using a message passing interface called SYNCEX[†].

The AVCS and TSWIFT codes use similar numerical algorithms; both solve the Reynolds-averaged Navier-Stokes equations on body-fitted grids using an explicit, finite-difference scheme. The codes include viscous terms in all grid directions, except that TSWIFT neglects the mixed-derivative viscous terms containing derivatives in the predominantly streamwise grid direction. The discretized equations are solved with a multi-stage Runge-Kutta time-marching scheme using a spatially varying time step, implicit residual smoothing, and preconditioning [6-9]. All simulations discussed herein were run using a 2-stage Runge-Kutta scheme with a CFL number of 2.5, and using the AUSM+ upwind scheme [10].

The TSWIFT code was derived from, and has the same basic features as, the SWIFT code [11] developed by Chima at the NASA Glenn Research Center. TSWIFT also has a fairly general multiblock capability (when used with SYNCEX), includes the two-equation SST turbulence model developed by Menter [12], and implements Giles' two-dimensional, steady-state, non-reflecting boundary conditions [13-14] at flow inlet, exit, and mixing-plane boundaries[‡]. Note that when a two-equation turbulence model is used, either the Wilcox k-ω model [15] or the Menter SST model, it is necessary to pitchwise average the computed turbulence properties on the upstream side of the mixing plane. In that case the turbulence kinetic energy, k, and the ratio of turbulence kinetic energy to turbulence dissipation rate, k/ω, are each mass-averaged, and the resulting average values of k and (indirectly) ω are used as inflow boundary values for the domain on the downstream side of the mixing plane.

---

† SYNCEX (pronounced "sink-ex") enables two or more executing programs to efficiently exchange data on a single computer and/or over a network.

‡ The SMPI code also implements Giles' two-dimensional, steady-state, non-reflecting boundary conditions.

Computational Grids

Two-dimensional grid blocks for axisymmetric computational domains were generated using an algebraic method. In most cases the mesh was restretched using a Poisson partial differential equation (PDE) solver, otherwise known as an elliptic grid generator, producing grids with better boundary-normal node clustering and spacings, and generally good local orthogonality.

Three-dimensional grid blocks for blade row computational domains, except for rotor downstream extension H-grid blocks, were generated using a computer program called TTGRID, which is a modified version of TCGRID [16], a three-dimensional grid generator for turbomachinery developed by Chima at the NASA Glenn Research Center. TTGRID applies an elliptic PDE solver to the streamwise-pitchwise (blade-to-blade) mesh surfaces of blade row C- and H-grids.

The AVCS and TSWIFT codes always directly compute the viscous sublayer solution for turbulent boundary layers on solid walls; that is, wall functions are not used. It is important, therefore, that node spacings at solid walls be sufficiently small. At all hub and tip endwalls, a wall-normal nominal spacing of 0.0001 to 0.0003 inches, depending on location, was specified for grid generation, and at all blade/vane surfaces a wall-normal nominal spacing of 0.0002 inches was specified. Corresponding inner-variable wall distances, y_w^+, typically range between 1.0 and 3.0 at endwall surfaces, and 1.0 and 2.0 at blade surfaces.

More details with figures showing the various grid blocks for the ADP and SDT fan system computational domains, respectively, can be found in References 17 and 18. The grid blocks reported in these references are not identical to those used in this study, but they are generally very similar, with the exception of the ADP rotor blade grid block near the hub endwall. For the current investigation the blade is fully attached to the hub, while in the reference the blade-to-hub attachment involves a mid-chord trunnion with fore and aft clearance gaps. Grid block sizes for the ADP and SDT fan systems are summarized below in Tables 1 and 2, respectively.

Table 1: Computational Grid Blocks for ADP Fan System

Grid Block	Size (I × J × K)	Nodes
Inlet H-Grid	169 × 1 × 85	14,365
Nozzle H-Grid	169 × 1 × 85	14,365
Nacelle H-Grid	297 × 1 × 65	19,305
Far Field H-Grid	169 × 1 × 45	7,605
Rotor Upstream H-Grid	21 × 26 × 85	46,410
Rotor Blade C-Grid	193 × 49 × 85	803,845
Rotor Tip Clearance O-Grid	161 × 13 × 13	27,209
Rotor Downstream Core H-Grid	49 × 89 × 53	231,133
Rotor Downstream Bypass H-Grid	69 × 89 × 73	448,293
Core Inlet Guide Vane C-Grid	177 × 41 × 53	384,621
Fan Exit Guide Vane C-grid	193 × 45 × 73	634,005
Total All Grid Blocks	–––	2,631,156

Table 2: Computational Grid Blocks for SDT Fan System

Grid Block	Size (I × J × K)	Nodes
Inlet H-Grid	169 × 1 × 85	14,365
Nozzle H-Grid	169 × 1 × 85	14,365
Nacelle H-Grid	321 × 1 × 65	20,865
Far Field H-Grid	177 × 1 × 45	7,965
Rotor Upstream H-Grid	33 × 42 × 85	117,810
Rotor Blade C-Grid	217 × 49 × 85	903,805
Rotor Tip Clearance O-Grid	179 × 13 × 17	39,559
Rotor Downstream H-Grid	89 × 89 × 81	641,601
Fan Exit Guide Vane C-grid	209 × 45 × 73	686,565
Total All Grid Blocks	–––	2,446,900

Aerodynamic Simulations

All aerodynamic simulations were performed with air modeled as a perfect gas, and with the ratio of specific heats, γ, equal to 1.400. Far-field total/stagnation properties are normalized to SSL conditions, so all computed and post-processed solution results directly represent corrected values. The effects of flight Mach number and altitude are embedded in the unit Reynolds number specified for the computations. At the ADP cruise condition, corresponding to standard day flight at 30,000 feet and Mach 0.800, the unit Reynolds number[†] is 3.047E5 inches^{-1}. Similarly, for standard day flight at 30,000 feet and Mach 0.780, which is the SDT cruise condition, the unit Reynolds number is 3.008E5 inches^{-1}. Note that at the takeoff and approach conditions, corresponding to SSL flight at Mach 0.100, the effect of Mach number was ignored, so the SSL unit Reynolds number of 5.915E-05 inches^{-1} was specified[‡].

The effects of turbulence were modeled using the Menter SST turbulence model [12], with freestream turbulence at the upstream far-field computational boundary specified to be 0.5 percent, and turbulence (eddy) viscosity set equal to 2.0 times the molecular viscosity. The corresponding turbulence kinetic energy depends on the far-field Mach number. For the conditions at takeoff/approach, ADP cruise, and SDT cruise, respectively, the calculated values are as follows: 3.74E-07, 2.13E-05, and 2.03E-05 (dimensionless; multiply by the far-field stagnation speed-of-sound-squared to obtain a dimensional value).

Since the core duct downstream of the CIGV row in the ADP fan system was not modeled for the CFD simulations, it was necessary to specify static pressures at the exit boundary of the CIGV computational domain. This was done by setting the hub static pressure at a specified value, and using simple radial-equilibrium to compute the static pressure distribution from hub to tip. For the baseline takeoff and cruise operating points, hub static pressure was adjusted iteratively to achieve the desired system bypass ratio (BPR) for each operating point. For the corresponding morphed-blade cases however, the hub static pressure from the baseline case was used, so BPR varies somewhat between related cases.

Aerodynamic performance comparisons between baseline and corresponding morphed-blade configurations are made, as already mentioned, on the basis of equal fan system thrust[§]. This involves varying fan rotational speed for the morphed blade configuration, thereby changing the thrust level for that system. It is possible to iteratively vary the rotational speed so as to ultimately match the baseline thrust, but it is normally much faster and more computationally efficient to simulate only two cases having thrust levels near the baseline value, and then use linear

---

†   Unit Reynolds number is based on far-field total/stagnation properties and has dimensions of inverse-length. The length unit must be the same as that of the computational grid(s).

‡   At 30,000 feet and flight Mach 0.800, the total-pressure correction factor, δ, is 0.4529, and the total-temperature correction factor, θ, is 0.8955. At 30,000 feet and flight Mach 0.780, the total-pressure correction factor is 0.4441, and the total-temperature correction factor is 0.8904. At sea level and flight Mach 0.100, the total-pressure correction factor is 1.0006, and the total-temperature correction factor is 1.0020.

§   Thrust is calculated by integrating flow field properties on the boundaries of a control volume surrounding the fan system. Solid surface boundaries and flow boundaries are involved. Control volume boundaries located outside the computational domain contribute zero to the net thrust of the system.

interpolation or extrapolation to calculate the thrust-matched quantities. As would be expected, most of the resulting fan performance quantities such as mass flow rate, total-pressure ratio, and power, differ from corresponding baseline values, but the magnitudes are generally similar.

Quantitative performance comparisons are made using overall stage adiabatic efficiency since it reflects most of the significant performance-related differences inherent in the computed aerodynamic solutions. Regarding this, it should be noted that for the ADP fan system, stage efficiency applies only to the bypass stream. Also note that all adiabatic efficiency values as presented herein are relative to conditions upstream of the fan inlet, which means that fan inlet total-pressure losses are included in the fan efficiencies.

Two other important performance-related figures of merit for comparing the computed aerodynamic solutions are fan stall margin and noise. Although a quantitative assessment and comparison of these parameters is well beyond the scope of this investigation, some relevant qualitative discussions are provided below where appropriate.

The computational solutions for the ADP and SDT fans systems are presented and discussed next. For convenience, Table 3 summarizes the flight conditions considered for the two systems. Before proceeding, however, a couple of comments concerning the selected flight Mach numbers are appropriate. The first concerns the two cruise Mach numbers, both of which were originally specified to be 0.800. While initial CFD solutions showed this value to be good for the ADP system, it proved to be excessive for the SDT system, where shock waves generated on the outer nacelle surface were fairly strong and noticeably adverse to the boundary layer there. Consequently, the flight Mach number for the SDT system was reduce to Mach 0.780. The second comment concerns the takeoff and approach Mach number of 0.100. This value is related to experimental testing in the 9- by 15-foot Low Speed Wind Tunnel at the NASA Glenn Research Center, rather than to aircraft mission profile information.

Table 3: Summary of Flight Conditions for Aerodynamic Simulations

ADP Fan	SDT Fan
Cruise Mach 0.800 @ 30,000 ft	Cruise Mach 0.780 @ 30,000 ft
Takeoff Mach 0.100 @ Sea Level	Takeoff Mach 0.100 @ Sea Level
_____	Approach Mach 0.100 @ Sea Level

ADP Fan System at Cruise

Mach number contours for the computed flow field of the ADP baseline fan system at the cruise operating condition are shown in Figure 3, where the three-dimensional blade-row solutions have been mixed-out averaged in the pitchwise direction. Note that about half of the outer far-field domain has been cropped in the upper image, so the outer boundary is much farther away than might be inferred from the figure. Only the baseline flow field is shown since it also closely represents that of the morphed-blade configurations as well[†].

Table 4 below summarizes the different configurations computationally investigated for the ADP fan at the cruise condition. Included in the table are corrected fan mass flow rates and system bypass ratios. Corresponding fan rotor and fan stage performance quantities[‡] are shown in Table 5. In each table the red entries indicate values that are linearly extrapolated, based on system thrust, from the computed values. Some of the data in Table 5 has been graphed, as presented in Figure 4, where the bottom graph shows system thrust, and the top graph shows stage adiabatic efficiency, each versus percent rotational speed.

Table 4: ADP Fan Configurations at Cruise (Flight Mach 0.800)

Configuration[§]	Hub Reset Angle (degrees)	Tip Morph Angle (degrees)	Rotational Speed (percent)	Mass Flow Rate (lbm/sec)	Bypass Ratio
Baseline	-9.0	0.0	95.96	93.71	13.30
H-4.5 // M-05	-4.5	-5.0	99.00	93.70	13.88
	-4.5	-5.0	100.00	93.99	13.85
	-4.5	-5.0	98.22	93.47	13.90
H-4.5 // M-07	-4.5	-7.0	96.00	93.45	13.98
H-0.0 // M-10	0.0	-10.0	102.00	93.21	14.56
	0.0	-10.0	104.00	93.64	14.57
	0.0	-10.0	101.12	93.02	14.56

---

† The qualifications stated here apply to all other results of the same type, presented subsequently.

‡ Throughout this report, overall aerodynamic quantities are based on spanwise entropy-averaged flow field properties (an entropy-conserving method), except for system thrust, which is based on mixed-out-averaged flow field properties. Average spanwise quantities are based on pitchwise mixed-out-averaged flow field properties. Fan total-pressure ratio and adiabatic efficiency are relative to the inlet freestream condition, and therefore include total-pressure losses for the fan/engine inlet.

§ In all configuration labels for the ADP fan, the number following "H" indicates the hub reset angle, in degrees, and the number following "M" indicates the tip morph angle, in degrees.

Table 5: ADP Fan System Performance at Cruise (Flight Mach 0.800)

Configuration	Rotational Speed (percent)	Rotor Pressure Ratio	Rotor Adiabatic Efficiency	Fan Stage Pressure Ratio	Fan Stage Adiabatic Efficiency	Fan System Corrected Thrust (lbf)
Baseline	95.96	1.2822	0.9218	1.2826	0.8881	615.01
H-4.5 // M-05	99.00	1.2865	0.9084	1.2880	0.8760	624.92
	100.00	1.2911	0.9035	1.2924	0.8707	637.57
	98.22	1.2829	0.9122	1.2846	0.8801	615.01
H-4.5 // M-07	96.00	1.2836	0.9237	1.2853	0.8909	615.38
H-0.0 // M-10	102.00	1.2861	0.8896	1.2875	0.8578	622.95
	104.00	1.2932	0.8782	1.2945	0.8465	640.95
	101.12	1.2830	0.8946	1.2844	0.8628	615.01

In Table 4, the BPR of 13.30 for the baseline configuration was taken from the original design report [1], and so was predetermined. Information in the design report also gives a design-point corrected mass flow rate of 91.8 lbm/sec at a stage total-pressure ratio of 1.294. The mass flow rate for the CFD solution is 2.1 percent higher, with a lower stage total-pressure ratio of 1.283. Since the design-point flight Mach number is unknown to the author, it is very possible that this performance difference is due largely to a flight Mach number difference[†].

The efficiency graph in Figure 4 shows an almost linear relationship between fan stage efficiency and rotational speed. This is not a general characteristic, however, but is particular to this fan at this operating condition. It appears to be driven primarily by rotor near-tip total-pressure losses, where a shock/boundary-layer interaction intensifies as rotational speed increases. Corresponding spanwise distributions of rotor adiabatic efficiency are shown in Figure 5, which also includes a graph of rotor total-pressure ratio. As can be seen in Figure 5, there is a clear trend of decreasing efficiency near the tip as rotational speed increases. The shock/boundary-layer interaction producing this trend is shown in Figure 6, which shows Mach number contours for the rotor flow field at 85 percent of span, for two of the configurations simulated; namely, the baseline configuration and the -10 degree morphed-blade configuration. Examination of the two flow fields reveals that the suction surface boundary layer remains attached downstream of the shock wave for the baseline case, while for the morphed-blade case a substantial separation exists.

Referring again to Figure 4, as well as Table 5, it can be seen that the morphed-blade configuration involving a -4.5 degree hub reset and a -7.0 degree tip morph is best. This configuration has the same rotational speed as the baseline, with a slightly higher fan stage adiabatic efficiency (+0.003 for the bypass stream). Only near the hub, locally, is the efficiency substantially below that of the baseline configuration (see Figure 5). The worst configuration is the

---

† Table XII in Reference 1 indicates an inlet corrected flow rate of 97.2 lbm/sec at cruise Mach number 0.82.

one with a 0.0 degree hub reset and a -10.0 degree tip morph. From Figure 4 it seems reasonable to infer that the efficiency could be improved, that is for a configuration with a 0.0 degree hub reset, by increasing the magnitude of the tip morph angle, thereby lowering rotational speed. However, in order to match the baseline speed and efficiency, a tip morph angle of somewhere around -16.0 degrees would be needed, which is probably an impractical amount of blade morphing.

ADP Fan System at Takeoff

Mach number contours for the computed flow field of the ADP baseline fan system at the takeoff operating condition are shown in Figure 7. The fan mass flow rate for the computed solution is 78.50 lbm/sec at a BPR of 13.50, which agrees reasonably well with the measured flow rate of 79.20 lbm/sec at a BPR of 11.50. Adjusting the computed flow rate to roughly account for the difference in BPR, by assuming a fixed bypass flow, gives a fan mass flow rate of 79.44 lbm/sec, which is in closer agreement. Note that the higher BPR of 13.50 was selected for the present investigation because it is more consistent with the cruise/design value, and also because higher BPR conditions tend to make the fan system performance less sensitive to small BPR changes, such as occurs with morphed-blade configurations.

For the takeoff condition only a single ADP morphed-blade configuration was investigated. The fan configuration and performance data are summarized below in Tables 6 and 7, respectively. As earlier, red entries indicate values that have been linearly extrapolated, based on system thrust, from computed values. Notice that the hub reset angle of -4.5 degrees is the same as that investigated for cruise, the intent being that tip morph angle varies from -7.0 degrees at takeoff to +5.0 degrees at cruise. Graphs of key performance data from Table 7 are presented in Figure 8, the bottom graph showing system thrust, and the top showing stage adiabatic efficiency, each versus percent rotational speed. Related spanwise profiles of rotor total-pressure ratio and adiabatic efficiency are provided in Figure 9.

All the results for takeoff show the morphed-blade aerodynamic performance to be nearly the same as the baseline performance. The flat trend in adiabatic efficiency (see Figures 8 and 9) as rotational speed varies is quite different from the trend at cruise, and is due to the lack of any sensitive fluid dynamic mechanisms that would cause substantial changes in total-pressure loss. There is, however, a possible negative performance impact for the morphed-blade configuration; namely, a potential reduction in stall margin, depending on where rotor stall initiates.

Table 6: ADP Fan Configurations at Takeoff (Flight Mach 0.100)

Configuration	Hub Reset Angle (degrees)	Tip Morph Angle (degrees)	Rotational Speed (percent)	Mass Flow Rate (lbm/sec)	Bypass Ratio
Baseline	0.0	0.0	100.00	78.50	13.50
H-4.5 // M+05	-4.5	5.0	96.00	76.75	12.89
	-4.5	5.0	98.00	78.32	12.96
	-4.5	5.0	98.51	78.72	12.98

Table 7: ADP Fan System Performance at Takeoff (Flight Mach 0.100)

Configuration	Rotational Speed (percent)	Rotor Pressure Ratio	Rotor Adiabatic Efficiency	Fan Stage Pressure Ratio	Fan Stage Adiabatic Efficiency	Fan System Corrected Thrust (lbf)
Baseline	100.0	1.2808	0.9450	1.2847	0.9194	1336.8
H-4.5 // M+05	96.0	1.2631	0.9464	1.2660	0.9203	1263.7
	98.0	1.2755	0.9460	1.2785	0.9200	1321.9
	98.5	1.2787	0.9459	1.2817	0.9199	1336.8

Although not shown, for the takeoff condition the morphed blade has higher leading-edge flow incidence angles over much of the span, especially near the hub, and to a lesser extent at midspan. In Figure 10, blade surface pressure coefficient distributions for the morphed and baseline rotor blades at 32 percent of span are compared. The morphed-blade distribution shows greater forward aerodynamic blade loading (vertical distance between suction- and pressure-surface static pressures), which is indicative of the higher incidence angles and would be expected to correspond to less stall tolerance for that particular region of the blade span. It must be emphasized, however, that this may or may not be significant, depending on where along the span the rotor tends to stall initially. Furthermore, whether or not a decrease in stall margin is important or critical depends on available and required stall margin levels, both of which are beyond the scope of this study.

SDT Baseline Fan System at Cruise and Takeoff

Mach number contours for the computed flow field of the SDT baseline fan system at the cruise operating condition are shown in Figure 11, and similarly, contours for the takeoff operating condition are shown in Figure 12. No morphed-blade configurations were investigated for the cruise condition, which corresponds to the fan aerodynamic design point, but the computed solution provides baseline performance results that are useful as a reference. Also, comparisons between the cruise and takeoff results show how the baseline fan performance varies between the two operating points.

Computed results for the cruise condition can only be compared to design values because experimental testing has not been performed at that condition. From the CFD simulation for cruise, the corrected fan mass flow rate is 100.9 lbm/sec, with a corresponding stage total-pressure ratio of 1.451 and a stage adiabatic efficiency of 0.896. These results are in good agreement with reported design values [4,5]; specifically, a mass flow rate of 100.5 lbm/sec at a stage pressure ratio of 1.470. It might be noted that the flight Mach number for the design-point cruise condition is not exactly known, so it may differ somewhat from that used for the simulation. In view of the computed transonic flow over the outer nacelle surface (see Figure 11), it seems unlikely that the flight Mach number would be larger than the value of 0.780 selected for this study. A slightly lower Mach number would only bring the computed and design values into closer agreement.

For the takeoff condition, the computational results can be directly compared to experimental measurement values [5]. The agreement is generally good, although there are some notable inconsistencies. In particular, the computed and measured fan mass flow rates are in very good agreement, both being the same at 97.2 lbm/sec. Fan stage total-pressure ratio, however, differs significantly, at 1.483 for the computed solution, and 1.509 from the measurements. Corresponding stage adiabatic efficiencies are 0.894 and 0.914, respectively. This apparent difference in stage pressure ratio is inconsistent with the agreement in mass flow rate, unless there is an error in the fan nozzle geometry model, which seems very unlikely considering the good agreement between CFD and design values at cruise. In any case, efforts to resolve and explain these performance discrepancies are beyond the scope of this investigation and would require detailed comparisons of the computational and available measurement data.

Spanwise distributions of SDT baseline rotor total-pressure ratio and adiabatic efficiency at the cruise and takeoff operating conditions are compared in Figure 13. From the total-pressure distributions it can be seen that rotor aerodynamic loading increases over only the outer three-fourths of the span, but especially at the tip, as flow rate decreases; that is, as fan pressure ratio increases from cruise to takeoff. Accompanying the increase in aerodynamic loading is a corresponding enlargement of the tip clearance secondary flow region where, as indicated by the adiabatic efficiency distributions, there is an increase in local total-pressure losses. From this performance trend the rotor can be expected to stall at its tip, which is not unusual and is significant to the current investigation.

SDT Fan System at Takeoff

Summarized below in Table 8 are the configurations investigated for the SDT fan at the takeoff condition, and in Table 9 the corresponding fan rotor and fan stage performance quantities are provided. As in previous tables, red entries indicate values that are linearly interpolated, based on system thrust, from the computed values. In Figure 14, graphs of the fan system thrust and the fan stage adiabatic efficiency, each versus percent rotational speed, are shown.

Table 8: SDT Fan Configurations at Takeoff (Flight Mach 0.100)

Configuration†	Tip Morph Angle (degrees)	Rotational Speed (percent)	Mass Flow Rate (lbm/sec)
Baseline	0.0	100.00	97.22
M+05	5.0	100.00	93.21
	5.0	105.00	97.52
	5.0	104.86	97.40

---

† In all configuration labels for the SDT fan, the number following "M" indicates the tip morph angle, in degrees.

Table 9: SDT Fan System Performance at Takeoff (Flight Mach 0.100)

Configuration	Rotational Speed (percent)	Rotor Pressure Ratio	Rotor Adiabatic Efficiency	Fan Stage Pressure Ratio	Fan Stage Adiabatic Efficiency	Fan System Corrected Thrust (lbf)
Baseline	100.00	1.4956	0.9134	1.4832	0.8935	2258.8
M+05	100.00	1.4443	0.9276	1.4337	0.9081	2051.0
	105.00	1.4942	0.9169	1.4822	0.8976	2264.5
	104.86	1.4928	0.9172	1.4809	0.8979	2258.9

In terms of overall adiabatic efficiency, the morphed-blade configuration represents a minor but significant improvement over the baseline, the difference being about 0.004. When the corresponding spanwise variations in rotor adiabatic efficiency and total-pressure ratio, shown in Figure 15, are considered, however, the performance differences are much more prominent. Notice in particular the change in spanwise aerodynamic loading, as represented by rotor total-pressure ratio, where for the morphed-blade configuration the loading at the outer one-third of span has been substantially reduced. Not only is the total-pressure ratio lower there, but the rotational speed is higher by 5 percent.

From an operational standpoint, this performance difference is potentially a major improvement, as it is almost certain to mean a much larger takeoff stall margin for the fan. Recall the earlier comment, made when comparing the baseline cruise and takeoff spanwise loading distributions, about SDT rotor stall occurring at the tip. Blade-to-blade flow field comparisons reinforce this conclusion. In Figure 16, for example, relative Mach number contours for the baseline and morphed-blade CFD solutions at 78 percent of span are compared, revealing substantially different bow and passage shock wave structures. For the baseline rotor the bow shock wave is fully detached and part of a strong "normal" shock that is located at the covered-passage entrance. In contrast, the bow shock wave for the morphed-blade rotor is only locally detached, with a weak oblique shock running into the covered passage, and the supersonic flow finally terminated by a "normal" passage shock located well within the covered passage. Consequently, the morphed-blade rotor can be expected to tolerate a much larger increase in downstream static pressure, and therefore also in rotor total-pressure ratio, before stall initiates in the tip region. Stall at the hub is not expected, because as already shown for this rotor at this operating condition, hub loading tends not to increase as overall aerodynamic loading increases (see Figure 13).

Another possible advantage of the morphed-blade rotor is related to the upstream-running weak oblique shock waves which, as can be seen from Figure 16, are much weaker compared to those of the baseline rotor. This might have a significant impact on upstream fan noise at takeoff. In the absence of an acoustic analysis, the potential is at least suggested by comparing the static pressure fields upstream of the rotor, near the grid boundary, as is done in Figure 17. In the figure, the pitchwise variations in static pressure near the rotor tip are easily seen to be greater and more extensive for the baseline flow field than for the morphed-blade flow field.

SDT Fan System at Approach

Mach number contours for the computed flow field of the SDT baseline fan system at the approach operating condition are shown in Figure 18. The different configurations investigated for the SDT fan at approach are summarized below in Table 10, and corresponding fan rotor and fan stage performance quantities are presented in Table 11. Again, as in previous tables, red entries indicate values that are linearly interpolated, based on system thrust, from computed values. Graphs of the fan system thrust and fan stage adiabatic efficiency, each versus percent rotational speed, are shown in Figure 19, and in Figure 20, graphs of corresponding spanwise distributions of rotor total-pressure ratio and adiabatic efficiency are shown.

Table 10: SDT Fan Configurations at Approach (Flight Mach 0.100)

Configuration	Tip Morph Angle (degrees)	Rotational Speed (percent)	Mass Flow Rate (lbm/sec)
Baseline	0.0	61.70	57.96
M+05	5.0	64.17	57.91
	5.0	64.79	58.47
	5.0	64.30	58.02
M+10	10.0	67.87	58.43
	10.0	67.44	58.04

Table 11: SDT Fan System Performance at Approach (Flight Mach 0.100)

Configuration	Rotational Speed (percent)	Rotor Pressure Ratio	Rotor Adiabatic Efficiency	Fan Stage Pressure Ratio	Fan Stage Adiabatic Efficiency	Fan System Corrected Thrust (lbf)
Baseline	61.70	1.1545	0.8933	1.1502	0.8699	715.20
M+05	64.17	1.1534	0.9138	1.1494	0.8908	711.99
	64.79	1.1566	0.9132	1.1526	0.8902	727.82
	64.30	1.1540	0.9137	1.1500	0.8907	715.20
M+10	67.87	1.1566	0.9223	1.1525	0.8992	726.20
	67.44	1.1544	0.9227	1.1503	0.8996	715.20

As can be seen both in Table 11 and in Figure 19, the blade morphing gives a relatively large increase in adiabatic efficiency; specifically, fan efficiency increases by about 0.02 and 0.03, respectively, for 5.0 and 10.0 degrees of tip morphing. Comparing in Figure 20 the different spanwise distributions of rotor adiabatic efficiency reveals that virtually all of the increase is achieved at the outer half of the span. These results are not surprising, and in fact were anticipated, because the outer-span blade aerodynamics for the baseline SDT rotor at the approach operating point involve high incidence angles, with a leading-edge boundary layer separation on the suction side of the blade. Although the boundary layer reattaches, it remains relatively thick. Tip morphing reduces the local incidence and aerodynamic loading, and therefore the size and severity of the separation, resulting in thinner suction surface boundary layers. To show this, blade-to-blade contour plots of relative Mach number for the baseline and 10.0 degree tip-morph rotor solutions at 75 percent of span are provided in Figure 21. In the figure, the differences in leading-edge flow incidence and suction surface boundary thickness are apparent. Note that the flow field solution for 5.0 degrees of tip morphing is, as might be expected, intermediate between the two solutions represented in Figure 21.

Finally, referring again to Figure 20, the spanwise distributions in rotor total-pressure ratio, when considered along with the differences in rotational speed, show a dramatic decrease in rotor tip aerodynamic loading as the amount of tip morphing increases. In general, larger tip morph angles (more blade twist) with higher rotational speeds increase the total-pressure ratio at the hub and lower it at the tip, while the overall total-pressure ratio remains about the same. The effect of this loading change should be a substantial increase in stall margin at approach, especially in view of the decreased tip incidence angles and improved suction surface aerodynamics that accompany the reduction in loading.

Concluding Remarks

The results of this preliminary investigation confirm that rotor blade morphing could be a useful technology, with the potential to enable significant improvements in fan aerodynamic performance. Even though the study is very limited in scope and confined to simple geometric perturbations of two existing fan systems, the aerodynamic effectiveness of blade morphing is demonstrated by the configurations analyzed.

For the ADP fan system the basic objective was to determine if rotor blade morphing could serve as an acceptable aerodynamic replacement for variable-pitch blade restaggering, a feature of the baseline design. Two operating conditions were considered, cruise and takeoff. Baseline levels of adiabatic efficiency were achieved without difficulty at both conditions, and resulting aerodynamic qualities appear to be good. On the negative side, there is a possible reduction in stall margin at the takeoff condition, but time and resource constraints precluded further investigation. For perspective, it might be added that a variable-pitch rotor, especially one with very good aerodynamic performance like the ADP rotor, already has the benefit of "variable geometry", so performance improvement through blade morphing was not an objective.

The SDT fan system with its fixed-geometry rotor provided a realistic opportunity for aerodynamic improvement. Since the fan aerodynamic design point is at the cruise condition, improvements at the takeoff and approach operating points were sought, and to a large extent

achieved. At takeoff, a relatively small improvement in adiabatic efficiency was realized with blade morphing, but a very substantial increase in stall margin could be inferred from the computational results, as well as a potential reduction in upstream fan noise. At approach, relatively large increases in both adiabatic efficiency and expected stall margin were attained, with a substantially thinner boundary layer on the blade suction surface, and a much smaller separation bubble at the blade leading edge. The observed improvement in rotor flow quality, especially the thinner boundary layers and resulting wakes, might be expected to also possibly reduce broadband noise.

Despite the positive results of this investigation, the limitations involved should not be underestimated. This work provides only a glimpse of what might be gained through blade morphing when incorporated as part of an original fan design, where the fan must be integrated and optimized with the engine and aircraft. Even the aircraft mission profile could be affected since it is closely coupled to propulsion system performance over a wide range of operating conditions. From this perspective it seems possible, at least conceptually, that blade morphing might yield unanticipated benefits and/or lead to unexpected performance capabilities. If consideration is limited only to the fan itself, even then it seems likely that an original design incorporating blade morphing would better capitalize on the variability that morphing offers; that is, compared to the results from this limited investigation.

Finally, it is important to note that the selection of particular configurations for the present investigation implies nothing about the relative merits of the selected configurations versus other possible morphing schemes and/or applications. For example, the benefits of stator blade (or guide vane) morphing, compressor blade morphing, spanwise non-linear morphing, and blade camber morphing, to name a few, were not considered or studied in this work. Also, a less conventional, but potentially suitable application for blade morphing might be supersonic aircraft propulsion, where engine cycle variability is normally much greater than that needed for subsonic propulsion.

References

1. Hobbs, David E., Neubert, Robert J., Malmborg, Eric W., Philbrick, Daniel H., Spear, David A., "Low Noise Research Fan Stage Design," NASA Contractor Report (NASA internal use only; contains Pratt & Whitney proprietary data), March 1995.

2. Hobbs, David E., Neubert, Robert J., Malmborg, Eric W., Philbrick, Daniel H., Spear, David A., "Low Noise Research Fan Stage Design," NASA CR-195382, March 1995.

3. Jeracki, Robert J., "Comprehensive Report of Fan Performance From Duct Rake Instrumentation on 1.294 Pressure Ratio, 806 ft/sec Tip Speed Turbofan Simulator Models," NASA TM-2006-213863, February 2006.

4. Podboy, Gary G., Krupar, Martin J., Hughes, Christopher E., Woodward, Richard P., "Fan Noise Source Diagnostic Test — LDV Measured Flow Field Results," NASA TM-2003-212330 (also AIAA-2002-2431), July 2003.

5. Hughes, Christopher E., Jeracki, Robert J., Woodward, Richard P., "Fan Noise Source Diagnostic Test — Rotor Alone Aerodynamic Performance Results," NASA TM-2005-211681 (also AIAA-2002-2426), April 2005.

6. Chima, R. V., "Viscous Three-Dimensional Calculations of Transonic Fan Performance," in CFD Techniques for Propulsion Applications, AGARD Conference Proceedings No. CP-510, AGARD, Neuilly-Sur-Seine, France, February 1992, pp. 21-1 to 21-19 (also NASA TM-103800).

7. Chima, R. V., and Yokota, J. W., "Numerical Analysis of Three-Dimensional Viscous Flows in Turbomachinery," AIAA Journal, Vol. 28, No. 5, May 1990, pp. 798-806.

8. Tweedt, Daniel L., and Chima, Rodrick V., "Rapid Numerical Simulation of Viscous Axisymmetric Flow Fields," NASA TM-107103 (also AIAA-96-0449), November 1995.

9. Tweedt, Daniel L., Chima, Rodrick V., and Turkel, Eli, "Preconditioning for Numerical Simulation of Low Mach Number Three-Dimensional Viscous Turbomachinery Flows," NASA TM-113120 (also ICOMP-97-11 and AIAA-97-1828), October 1997.

10. Chima, R. V. and Liou, M.-S., "Comparison of the AUSM+ and H-CUSP Schemes for Turbomachinery Applications," AIAA Paper AIAA-2003-4120 (also NASA TM-2003-212457), June 2003.

11. Chima, R. V., "Swift – Multiblock Analysis Code for Turbomachinery, User's Manual and Documentation," Version 300, August 2003.

12. Menter, R. F., "Two-Equation Eddy-Viscosity Turbulence Models for Engineering Applications," AIAA Journal, Vol. 32, No. 8, August 1994, pp. 1598-1605 (also NASA TM-111958).

13. Giles, Michael B., "Nonreflecting Boundary Conditions for Euler Equation Calculations," AIAA Journal, Vol. 28, No. 12, December 1990, pp. 2050-2058.

14. Giles, Michael, "UNSFLO: A Numerical Method For The Calculation Of Unsteady Flow In Turbomachinery," GTL Report No. 205, May 1991, pp. 45-56.

15. Wilcox, David C., *Turbulence Modeling for CFD*, DCW Industries, Inc., La Cañada, CA, Third Edition, 2006.

16. Chima, R. V., "TCGRID 3-D Grid Generator for Turbomachinery, User's Manual and Documentation," Version 300, July 2003.

17. Tweedt, Daniel L., "Computational Aerodynamic Simulations of an 840 ft/sec Tip Speed, Advanced Ducted Propulsor Fan System Model for Acoustic Methods Assessment and Development," NASA CR to be published, March 2012.

18. Tweedt, Daniel L., "Computational Aerodynamic Simulations of a 1215 ft/sec Tip Speed Transonic Fan System Model for Acoustic Methods Assessment and Development," NASA CR to be published, March 2012.
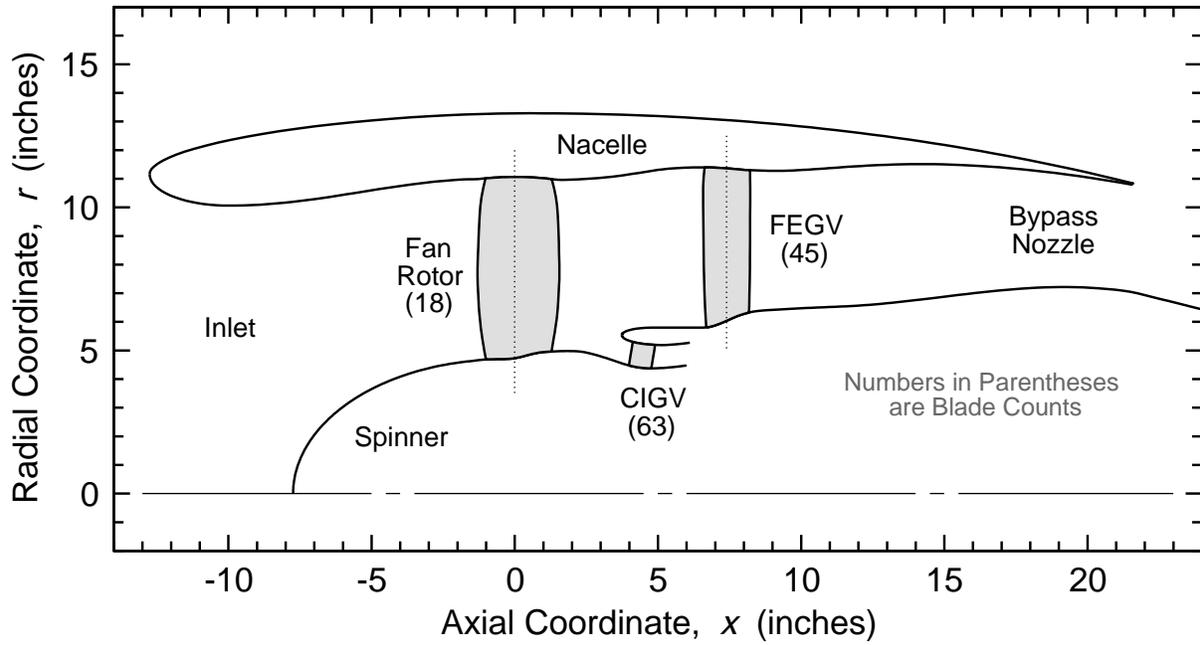
Figure 1: Meridional-Plane Drawing of ADP Fan System
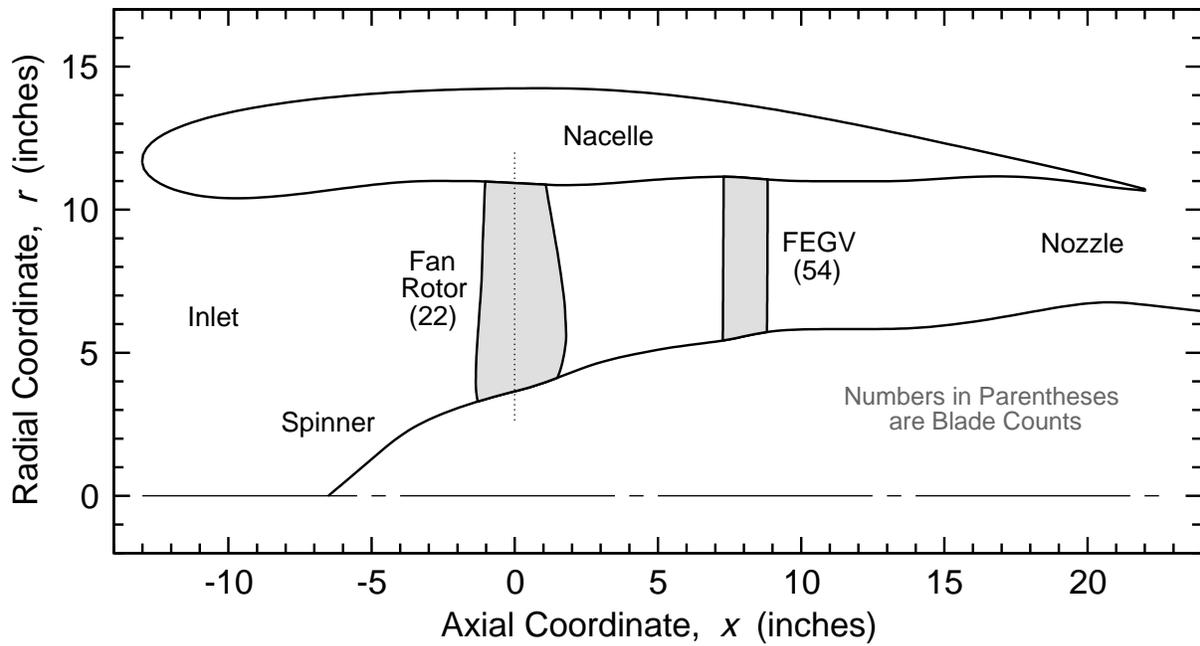
Figure 2: Meridional-Plane Drawing of SDT Fan System

ADP Baseline Fan System at Cruise Condition
Pitchwise-Averaged Flow Field
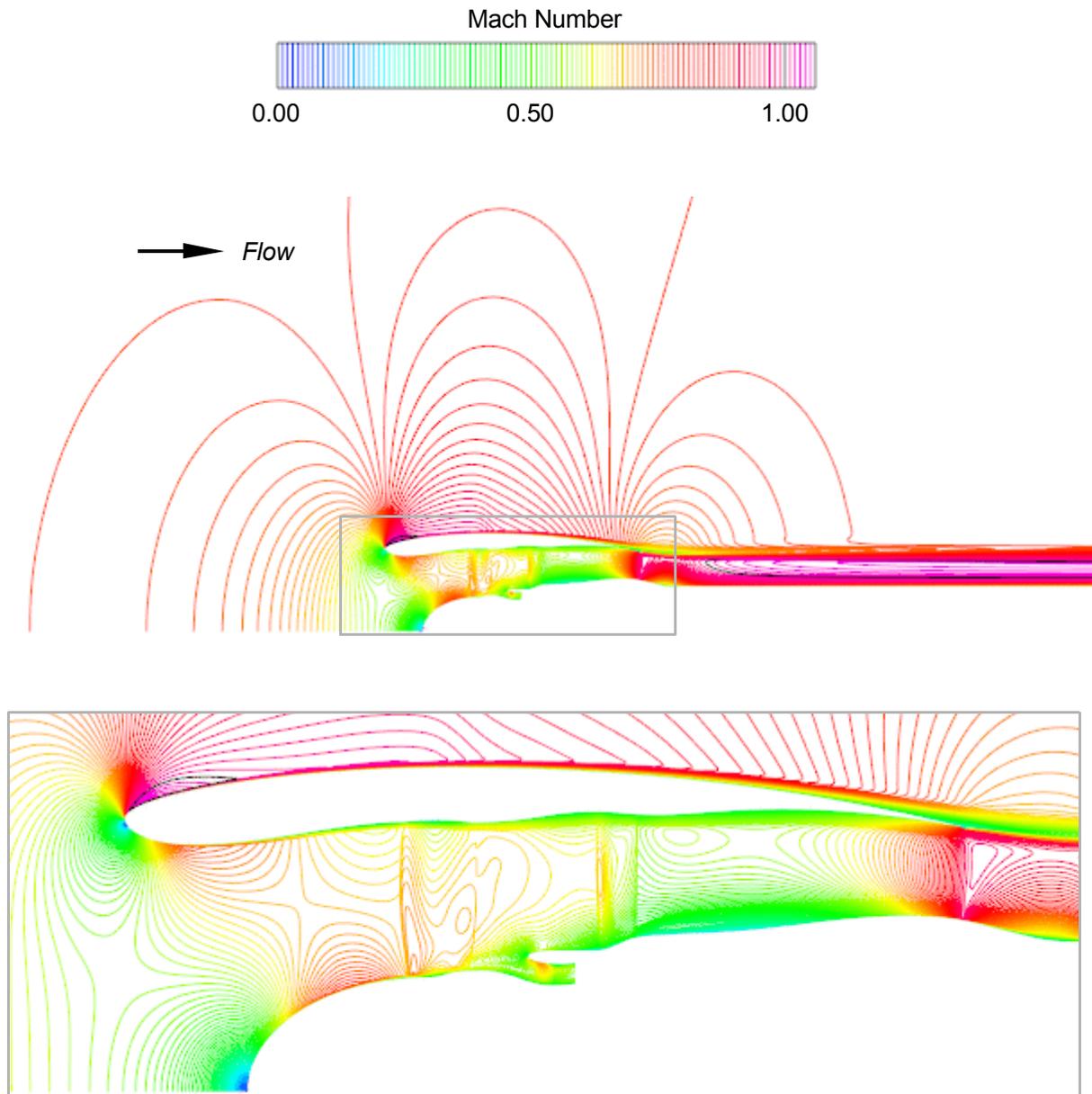
*Figure 3: Computed Flow Field for ADP Baseline Fan System at Cruise;
Pitchwise-Averaged Flow; Mach Number Contours*
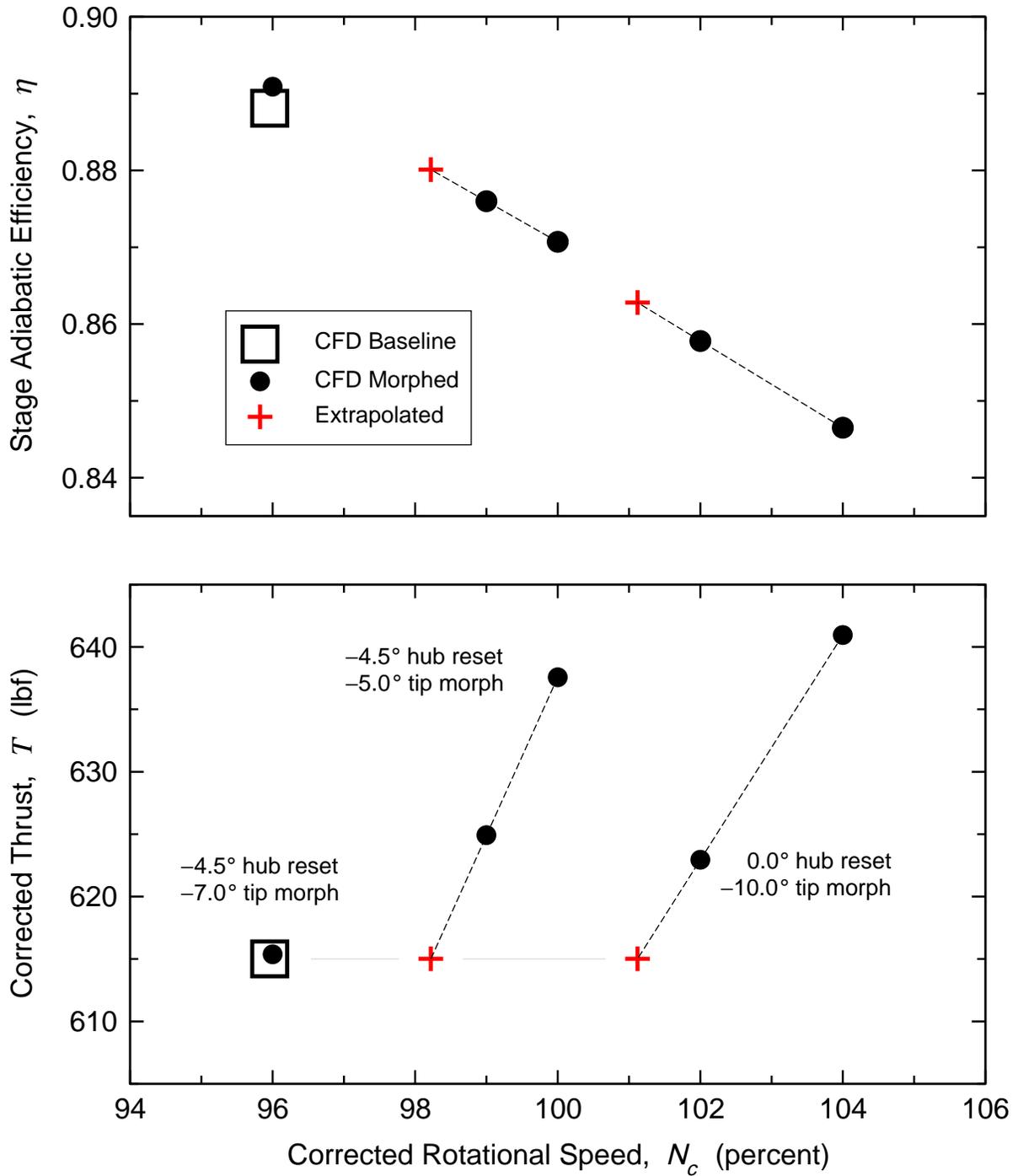
Figure 4: Overall Performance of ADP Fan System at Cruise

ADP Rotor at Cruise Condition
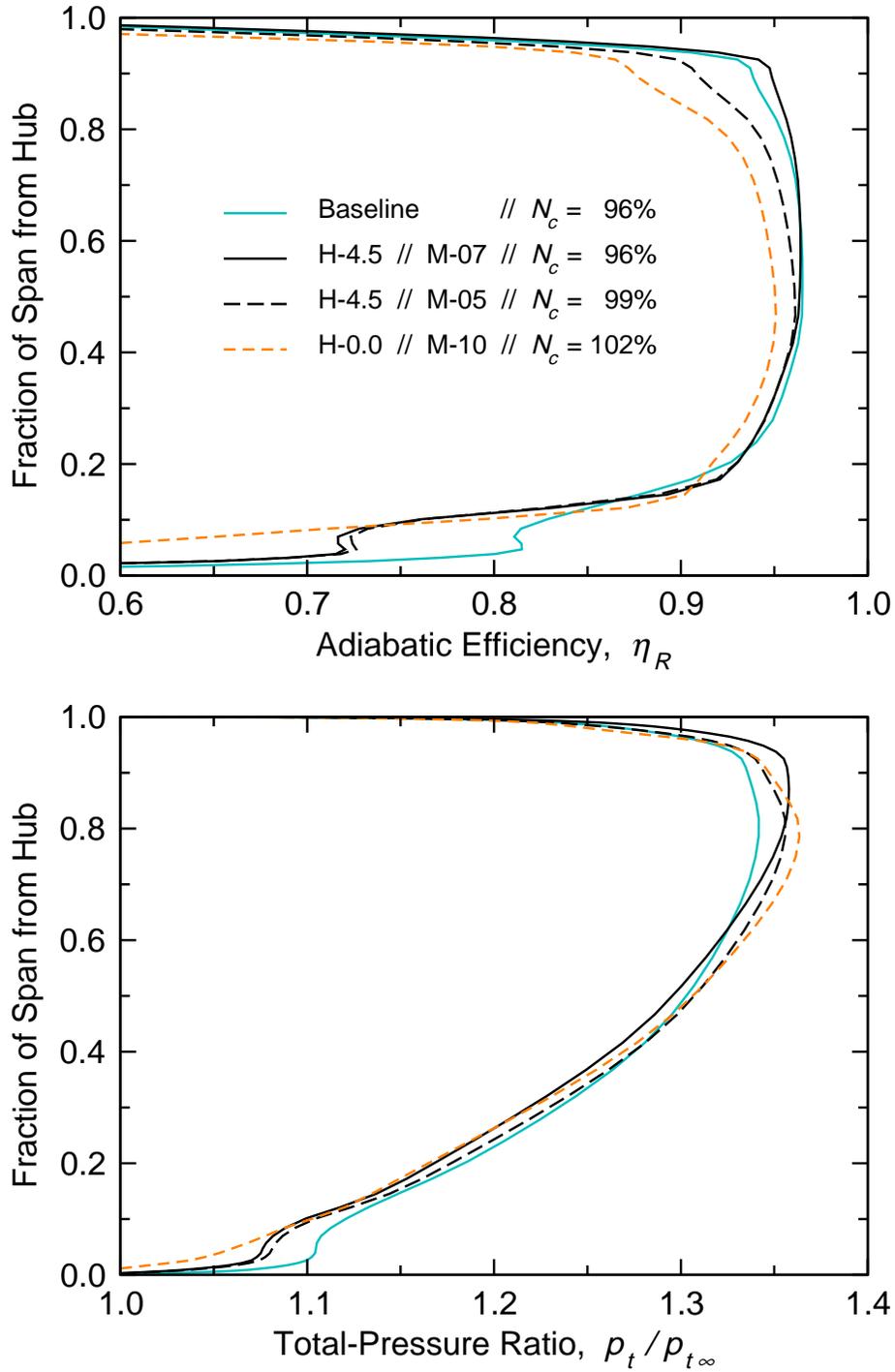
Figure 5: Spanwise Distributions of ADP Rotor Total-Pressure Ratio and Adiabatic Efficiency at Cruise

ADP Rotor at Cruise Condition
85 Percent of Span from Hub
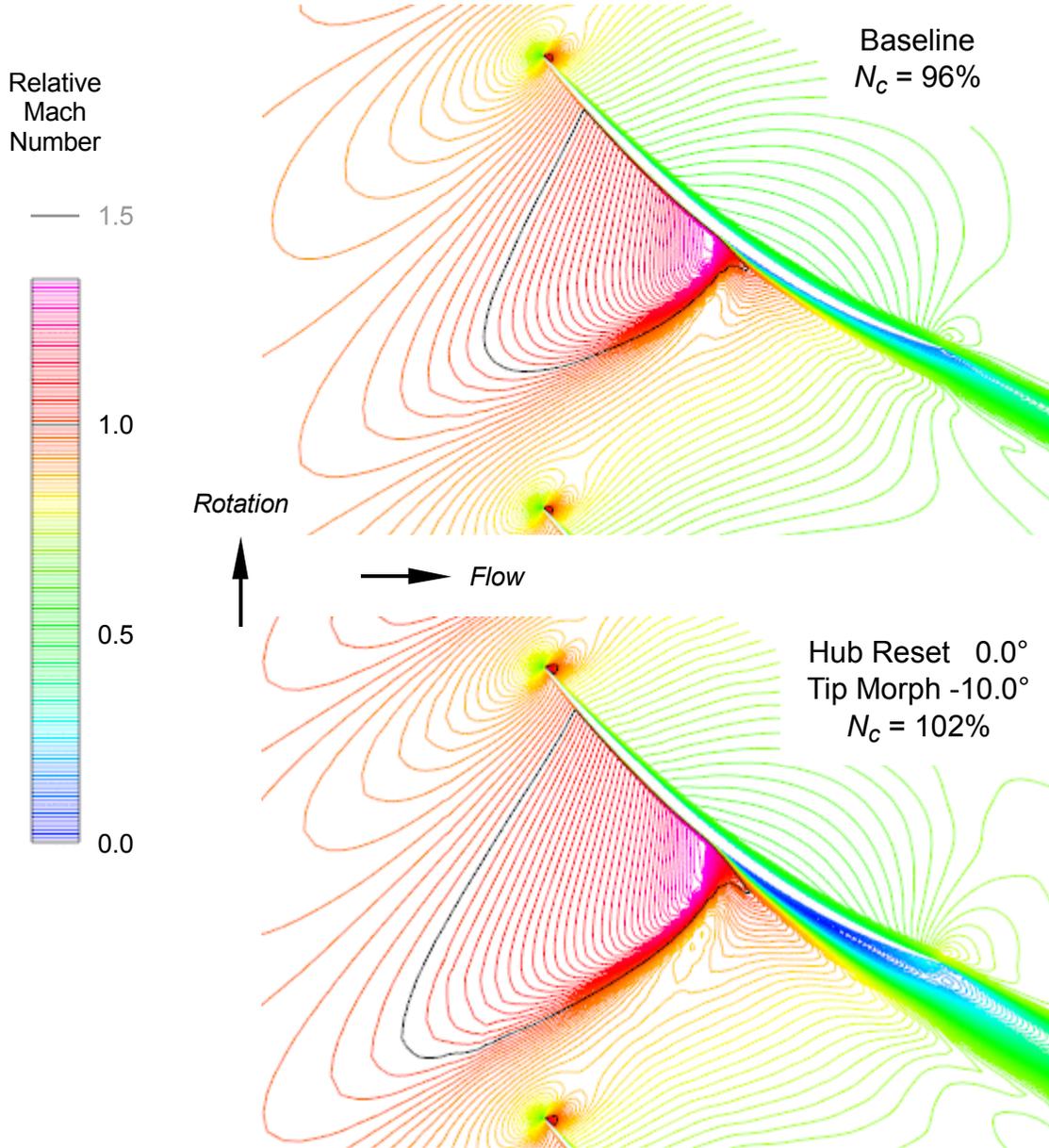
Figure 6: Computed Blade-to-Blade Flow Fields for ADP Rotor at Cruise; 85 Percent of Span; Relative Mach Number Contours

ADP Baseline Fan System at Takeoff Condition
Pitchwise-Averaged Flow Field
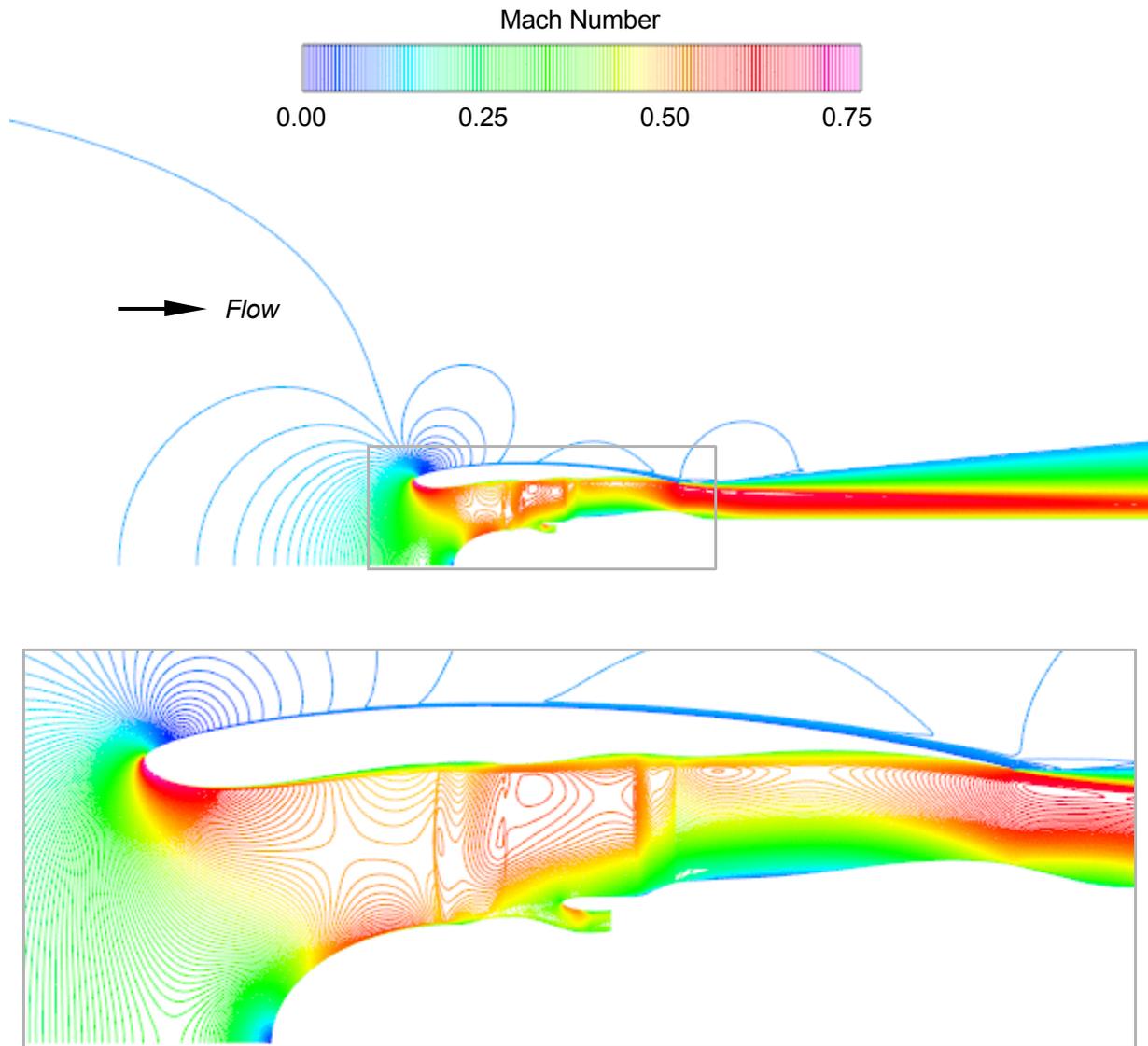
Figure 7: Computed Flow Field for ADP Baseline Fan System at Takeoff;
Pitchwise-Averaged Flow; Mach Number Contours

ADP Fan at Takeoff Condition
Flight Mach Number 0.100
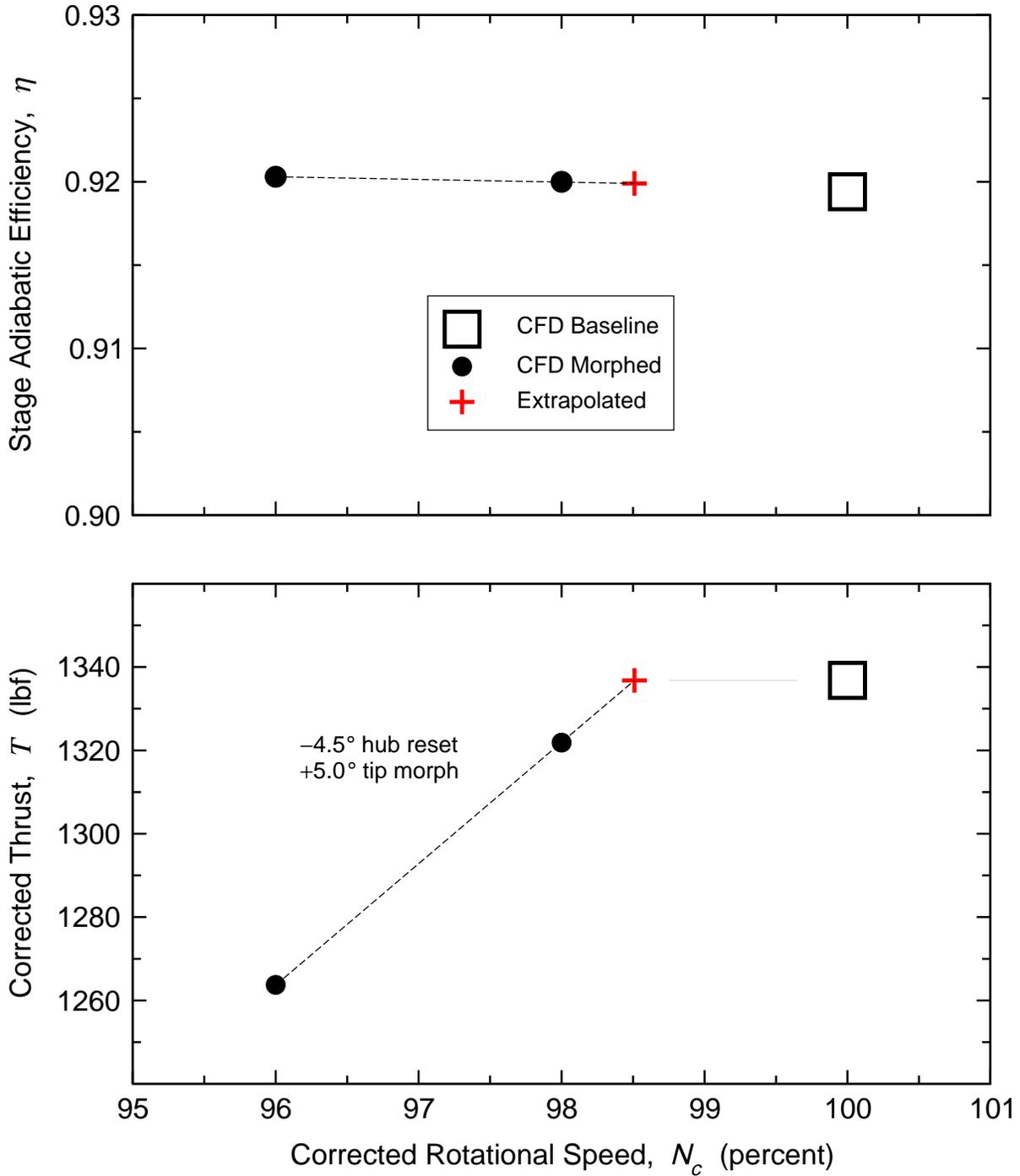
Figure 8: Overall Performance of ADP Fan System at Takeoff

ADP Rotor at Takeoff Condition
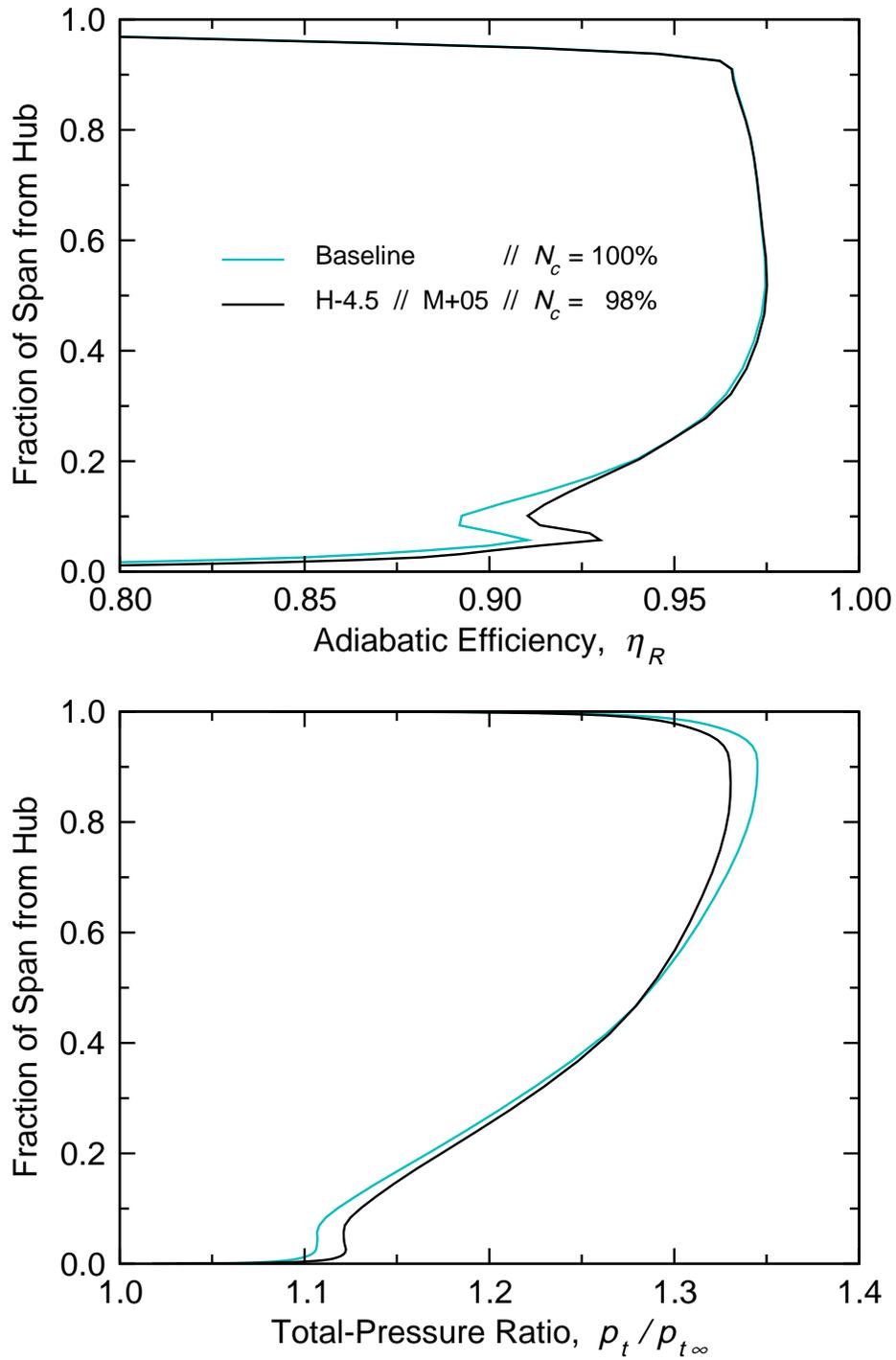
Figure 9: Spanwise Distributions of ADP Rotor Total-Pressure Ratio and Adiabatic Efficiency at Takeoff
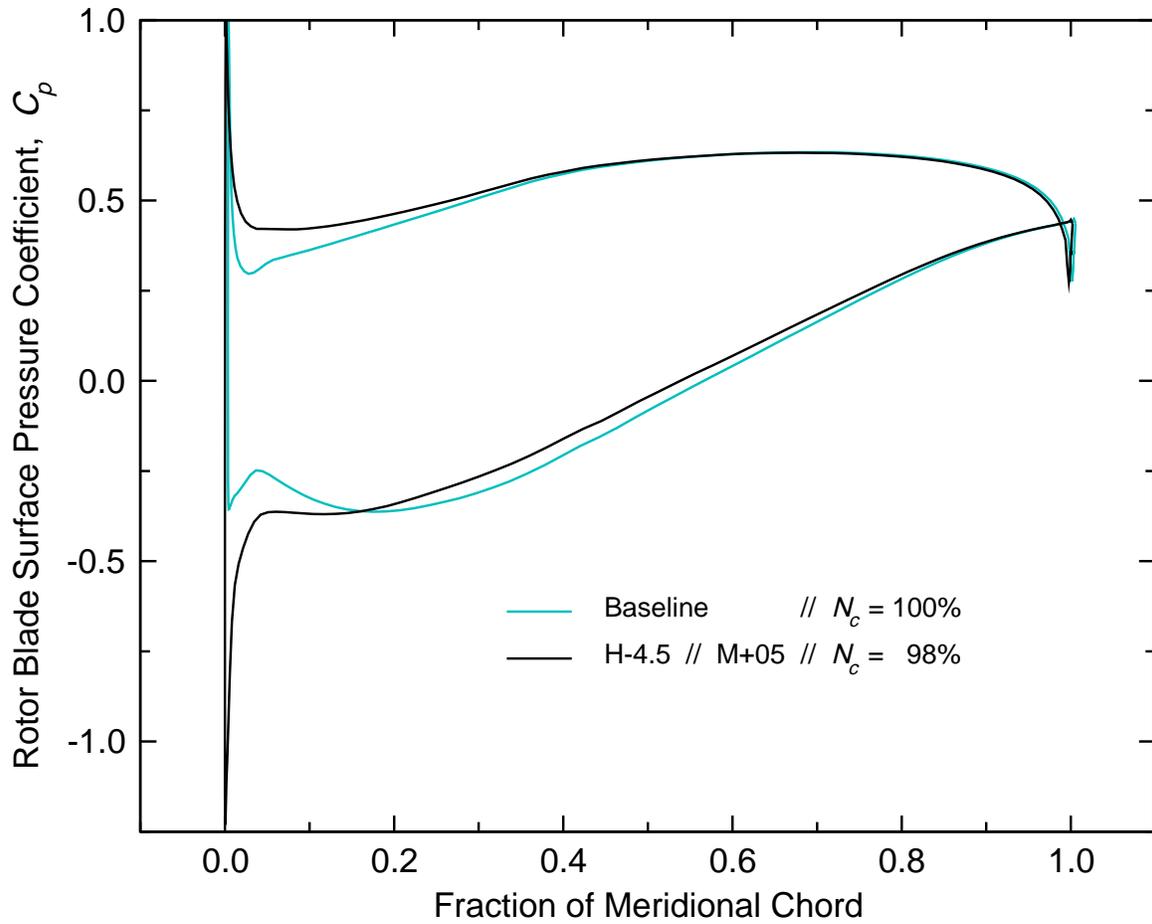
Figure 10: Blade Surface Pressure Coefficient Distributions for ADP Rotor at Takeoff; 32 Percent Span

SDT Baseline Fan System at Cruise Condition
Pitchwise-Averaged Flow Field
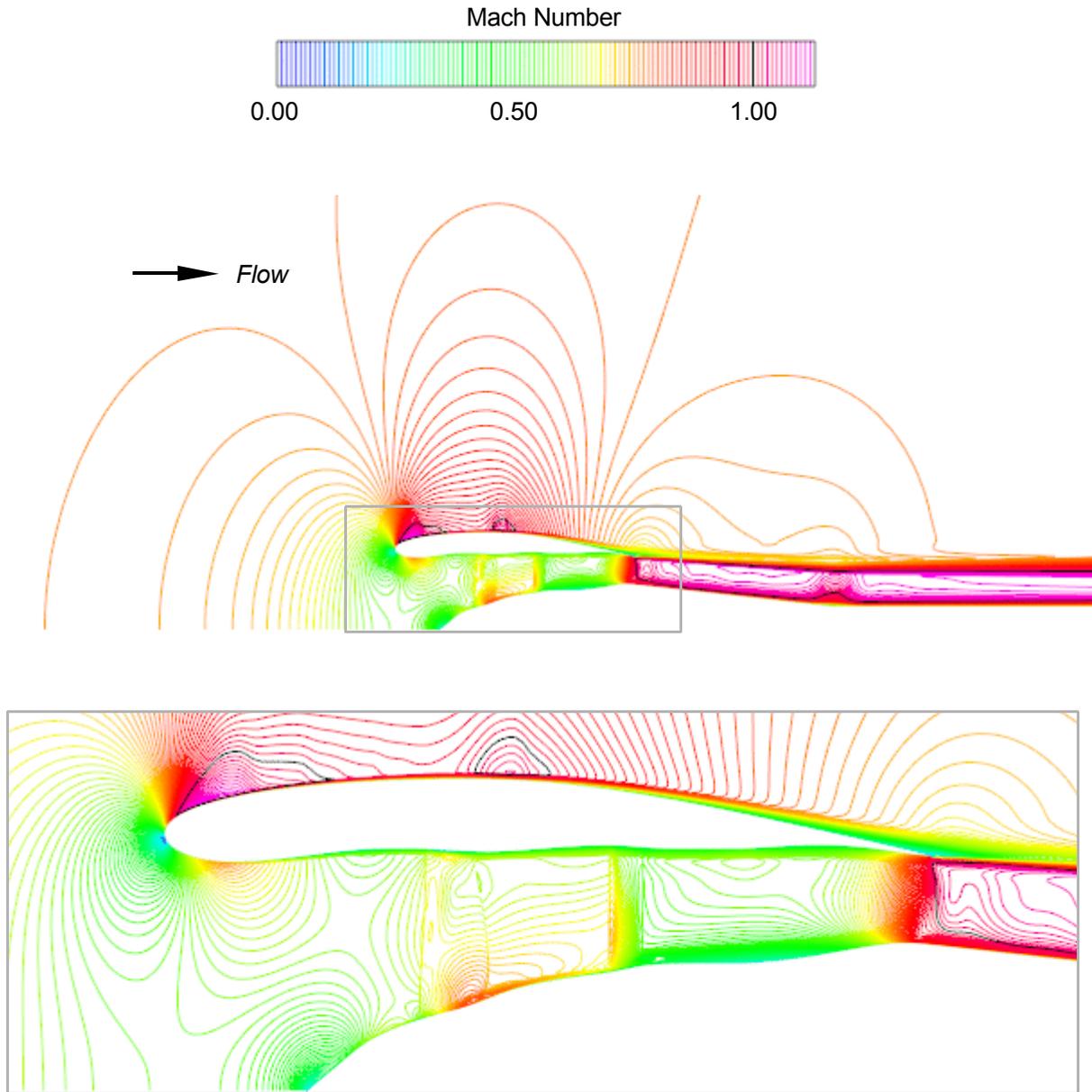
*Figure 11: Computed Flow Field for SDT Baseline Fan System at Cruise;
Pitchwise-Averaged Flow; Mach Number Contours*

SDT Baseline Fan System at Takeoff Condition
Pitchwise-Averaged Flow Field
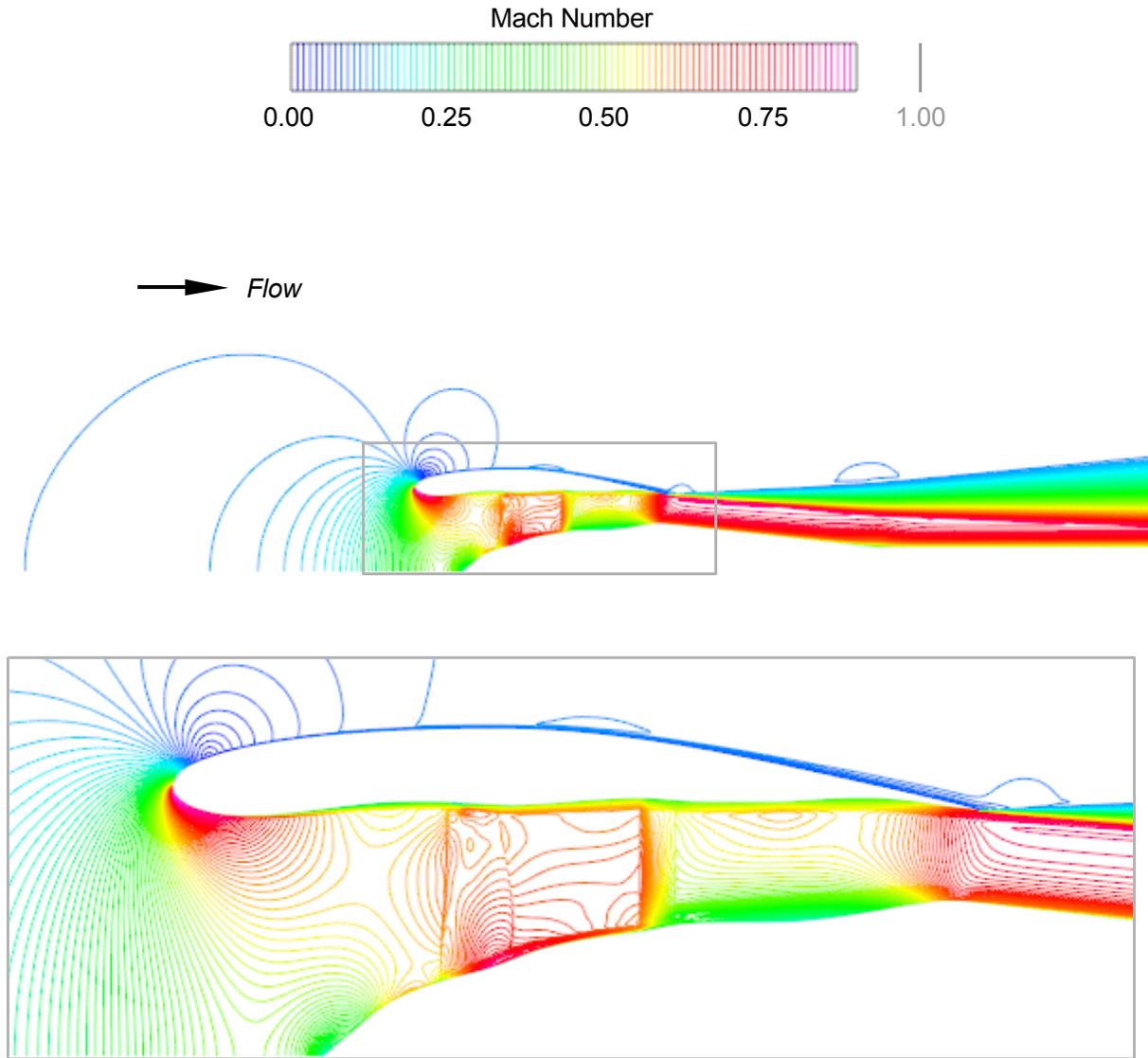
Mach Number

Figure 12: Computed Flow Field for SDT Baseline Fan System at Takeoff;
Pitchwise-Averaged Flow; Mach Number Contours

SDT Baseline Rotor at Design Rotational Speed
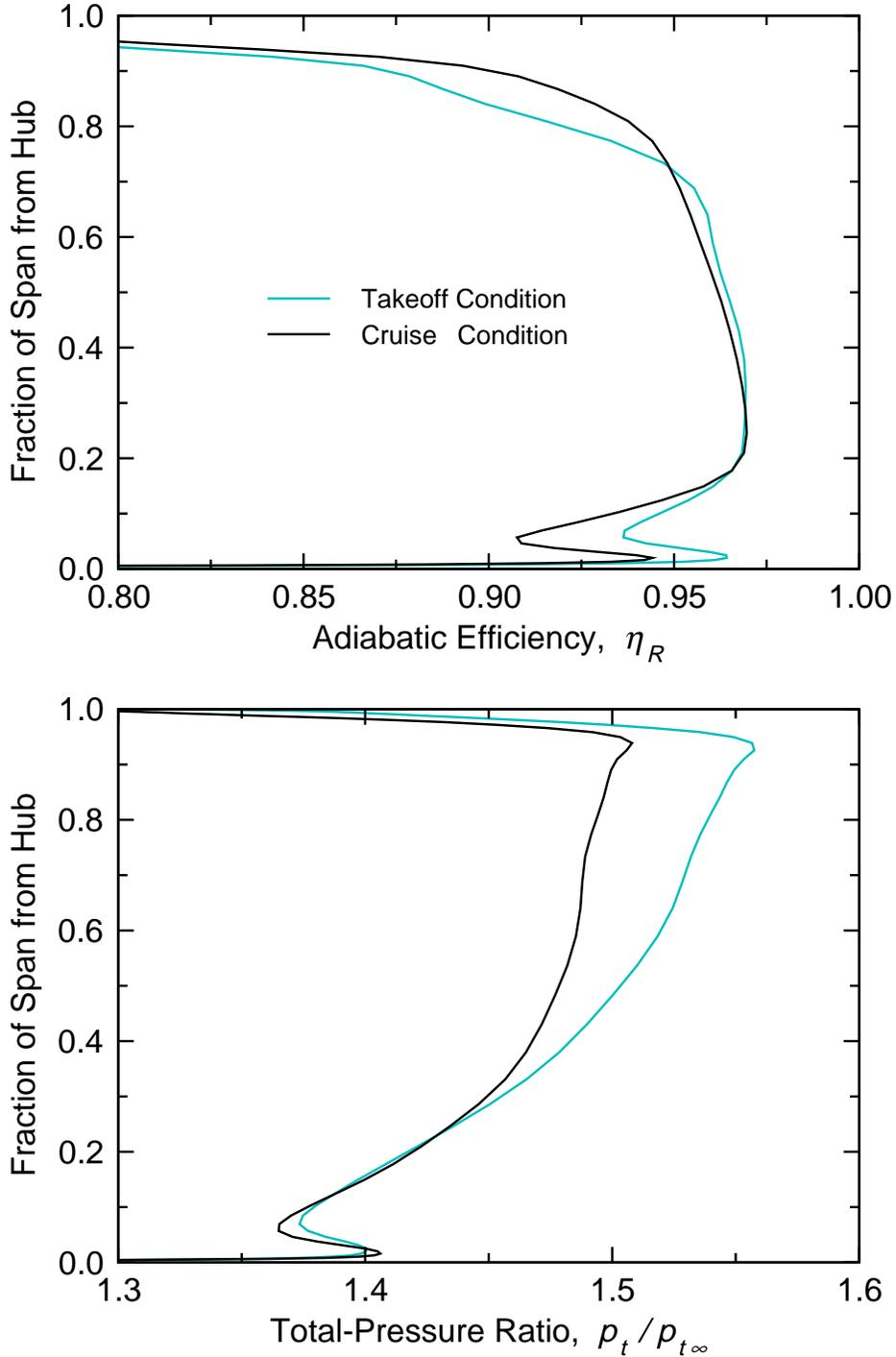
Figure 13: Spanwise Distributions of SDT Baseline Rotor Total-Pressure Ratio and Adiabatic Efficiency at Cruise and Takeoff

Figure 14: Overall Performance of SDT Fan System at Takeoff

SDT Rotor at Takeoff Condition
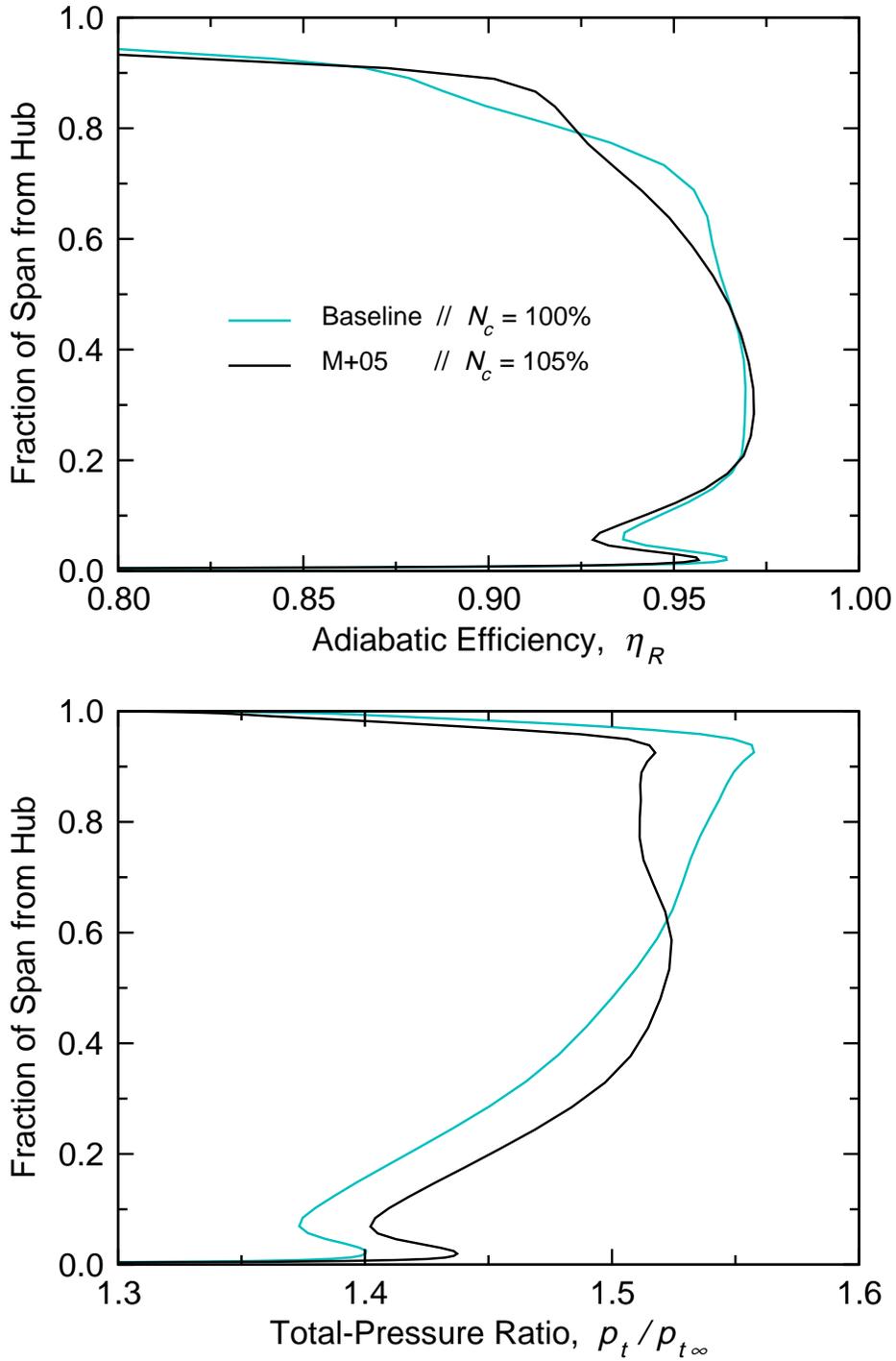
*Figure 15: Spanwise Distributions of SDT Rotor Total-Pressure Ratio
and Adiabatic Efficiency at Takeoff*

SDT Rotor at Takeoff Condition
78 Percent of Span from Hub
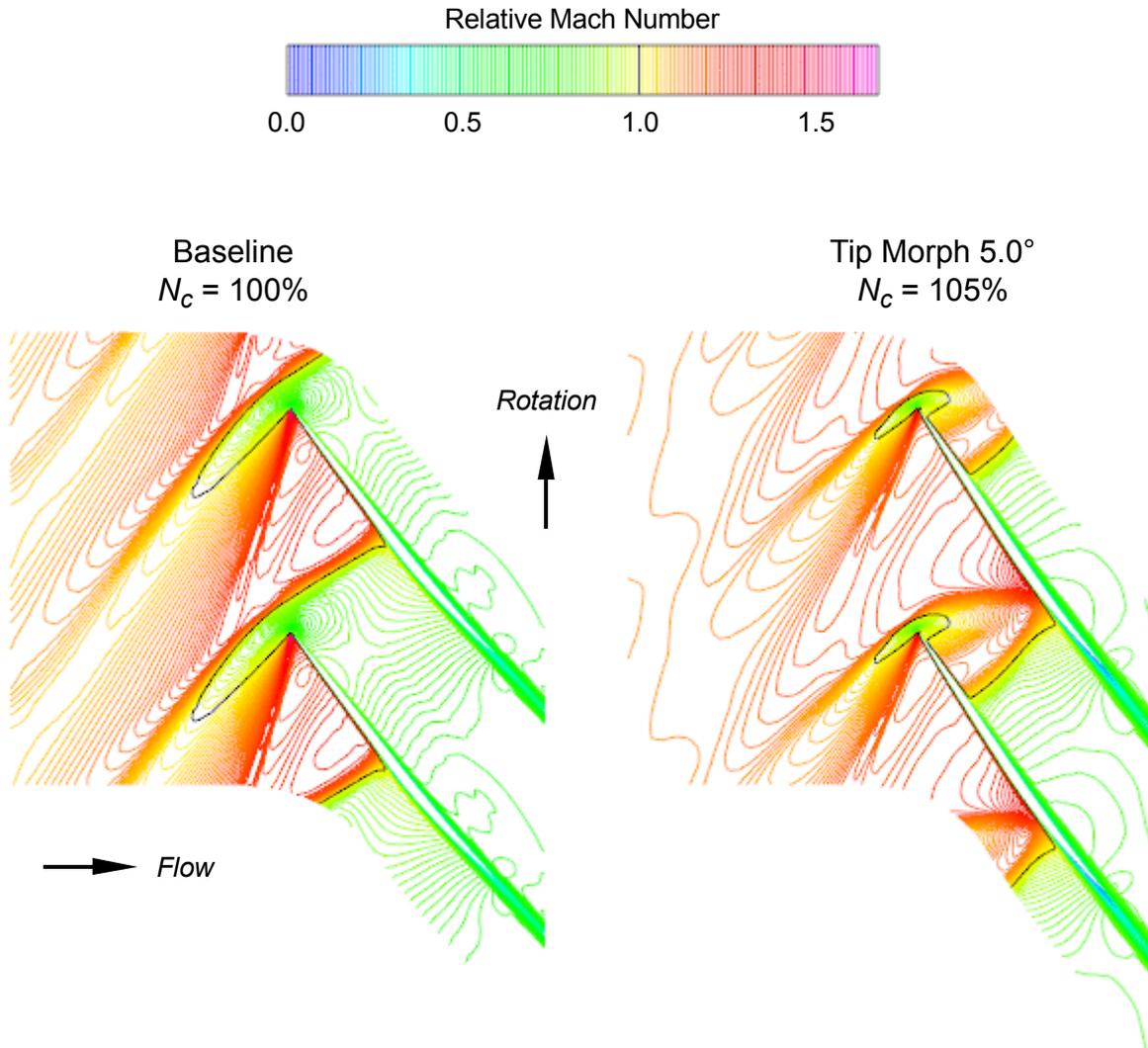
*Figure 16: Computed Blade-to-Blade Flow Fields for SDT Rotor at Takeoff;
78 Percent of Span; Relative Mach Number Contours*

SDT Rotor at Takeoff Condition
Rotor Upstream Static Pressure Field
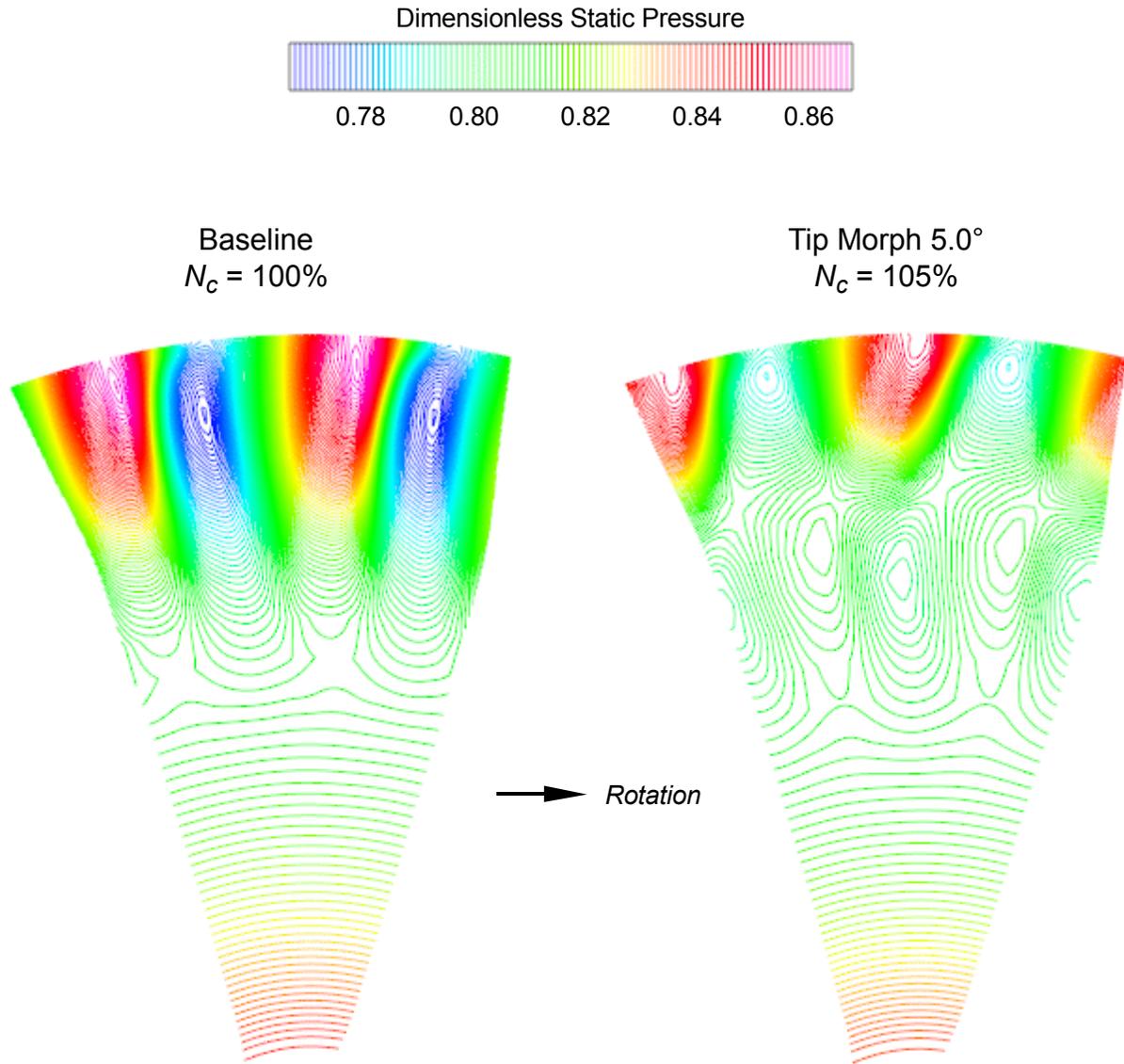
Figure 17: *Computed Static-Pressure Fields Upstream of SDT Rotor at Takeoff*

SDT Baseline Fan System at Approach Condition
Pitchwise-Averaged Flow Field
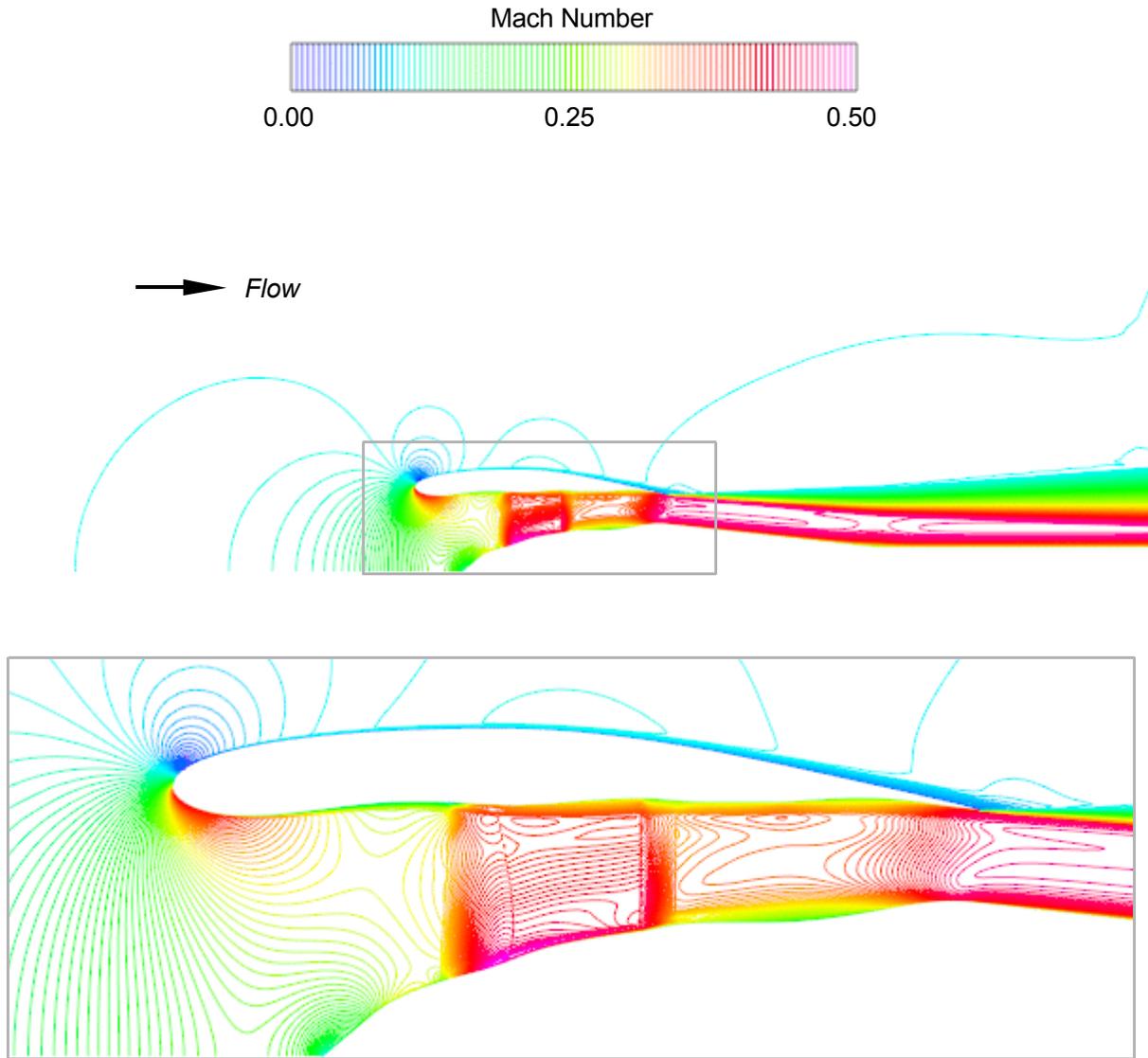
*Figure 18: Computed Flow Field for SDT Baseline Fan System at Approach;
Pitchwise-Averaged Flow; Mach Number Contours*

SDT Fan at Approach Condition

Flight Mach Number 0.100
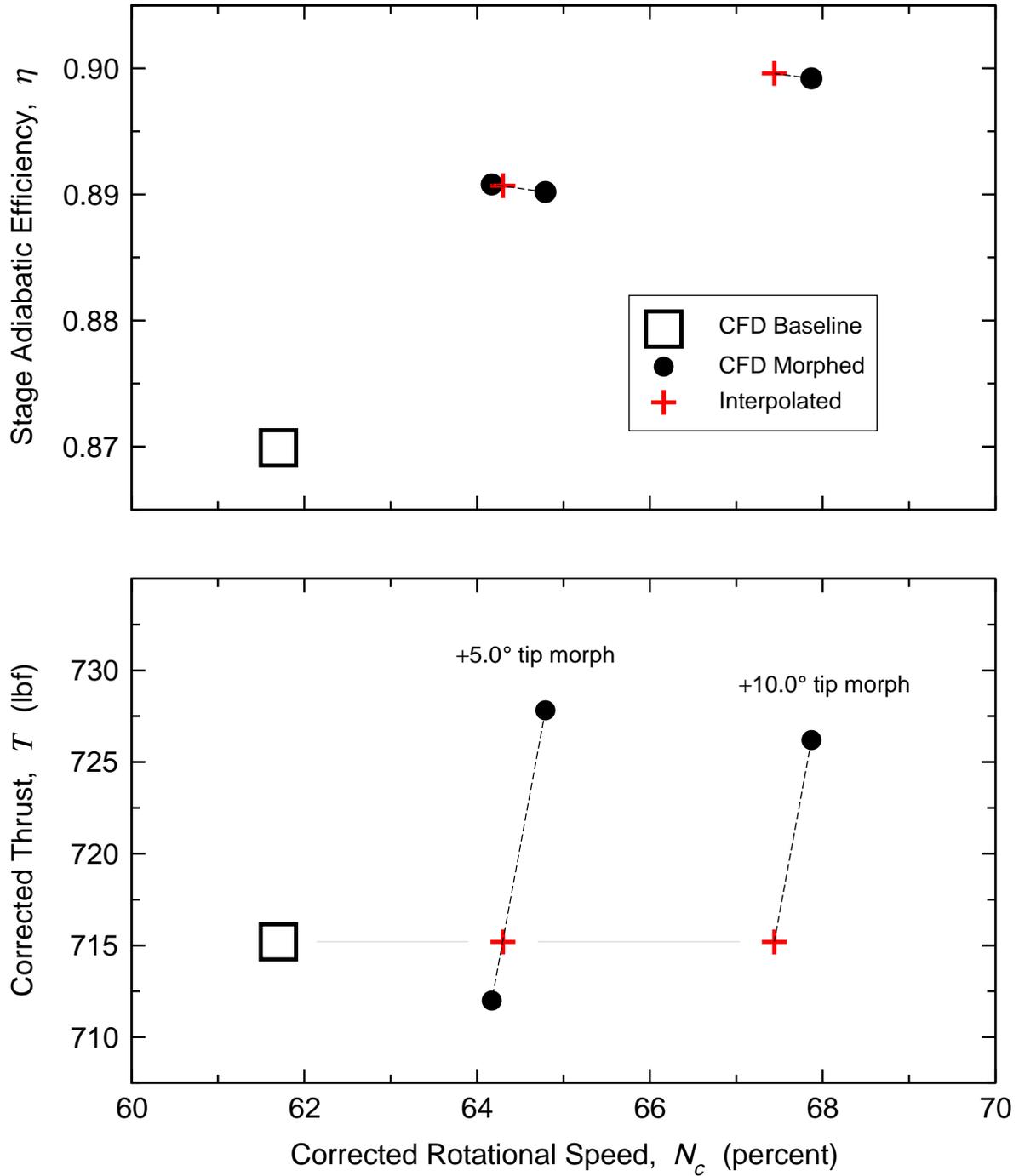
Figure 19: *Overall Performance of SDT Fan System at Approach*

SDT Rotor at Approach Condition

Legend:
- Baseline // $N_c = 61.7\%$
- M+05 // $N_c = 64.2\%$
- M+10 // $N_c = 67.9\%$

Adiabatic Efficiency, η_R

Total-Pressure Ratio, $p_t / p_{t\infty}$

Fraction of Span from Hub
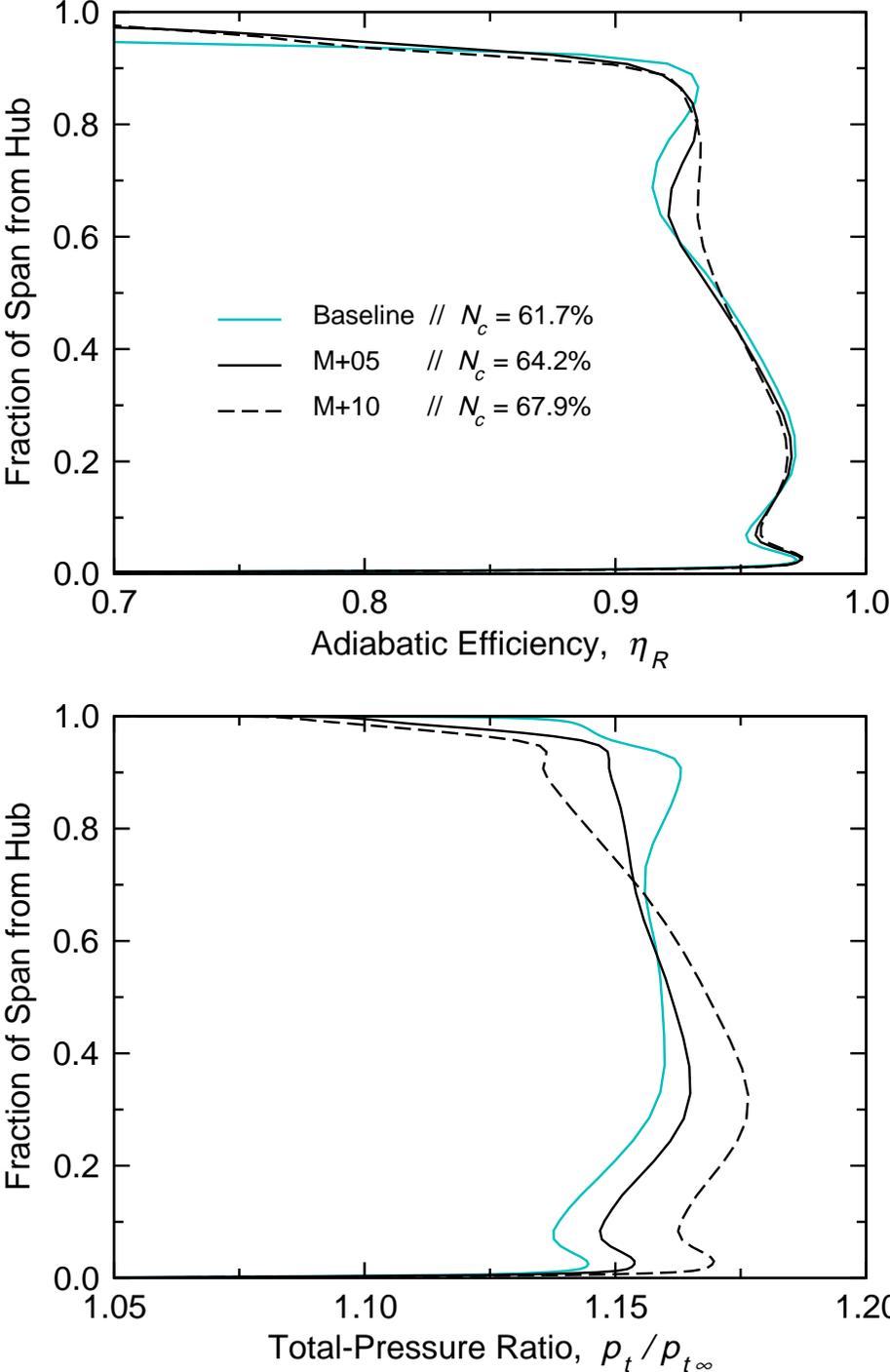
Figure 20: Spanwise Distributions of SDT Rotor Total-Pressure Ratio and Adiabatic Efficiency at Approach

SDT Rotor at Approach Condition
75 Percent of Span from Hub

Relative Mach Number

0.0   0.5   1.0

Baseline
N_c = 61.7%

Tip Morph 10.0°
N_c = 67.9%
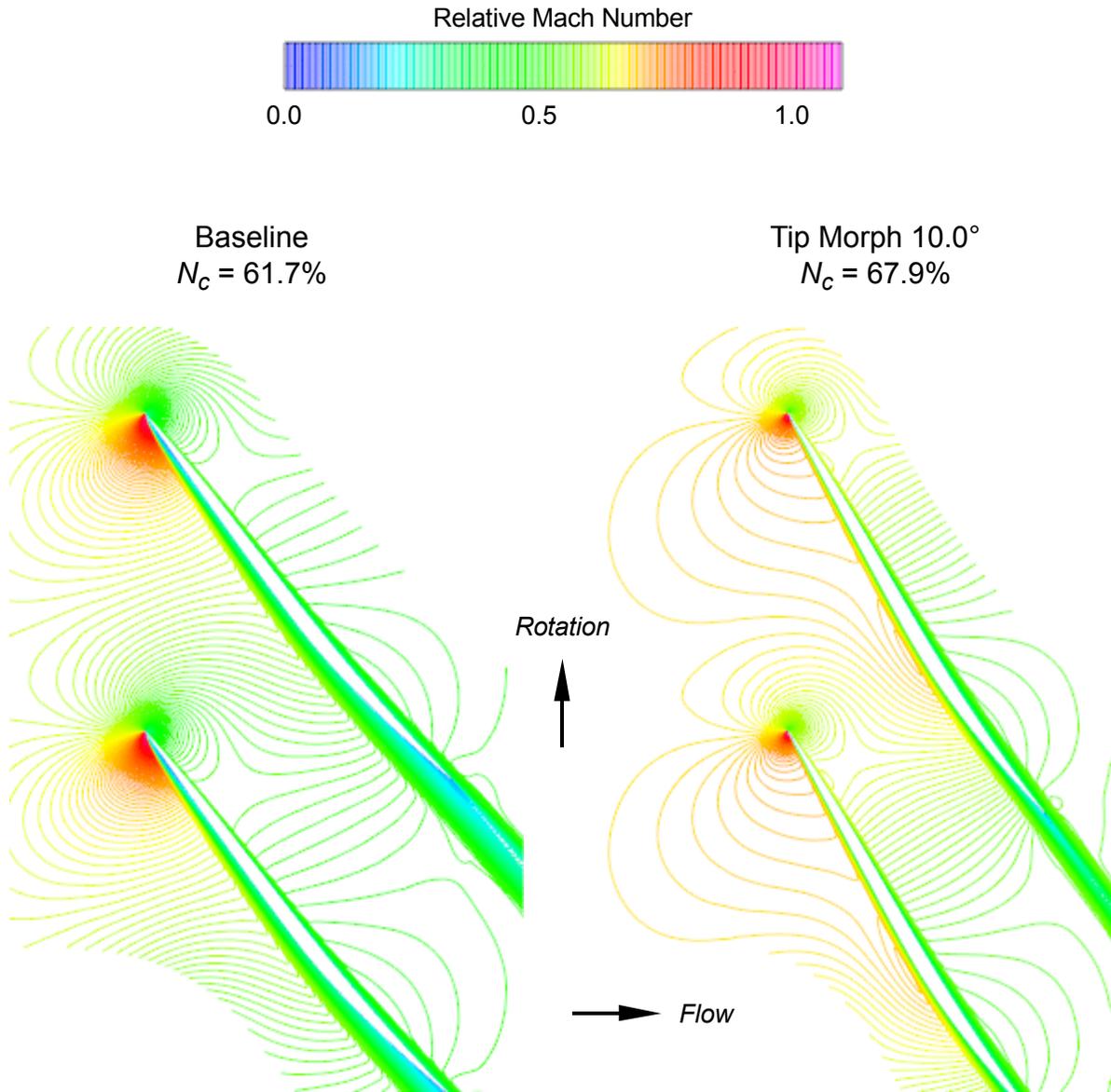
Rotation

Flow

Figure 21: Computed Blade-to-Blade Flow Fields for SDT Rotor at Approach;
75 Percent of Span; Relative Mach Number Contours

1. REPORT DATE *(DD-MM-YYYY)* 01-12-2012	2. REPORT TYPE Final Contractor Report	3. DATES COVERED *(From - To)*

4. TITLE AND SUBTITLE Preliminary Aerodynamic Investigation of Fan Rotor Blade Morphing	5a. CONTRACT NUMBER NNC06BA07B
	5b. GRANT NUMBER
	5c. PROGRAM ELEMENT NUMBER
6. AUTHOR(S) Tweedt, Daniel, L.	5d. PROJECT NUMBER
	5e. TASK NUMBER NNC10E541
	5f. WORK UNIT NUMBER WBS 473452.02.03.07.06.01.01

7. PERFORMING ORGANIZATION NAME(S) AND ADDRESS(ES) AP Solutions, Inc.	8. PERFORMING ORGANIZATION REPORT NUMBER E-18558

9. SPONSORING/MONITORING AGENCY NAME(S) AND ADDRESS(ES) National Aeronautics and Space Administration Washington, DC 20546-0001	10. SPONSORING/MONITOR'S ACRONYM(S) NASA
	11. SPONSORING/MONITORING REPORT NUMBER NASA/CR-2012-217815

12. DISTRIBUTION/AVAILABILITY STATEMENT
Unclassified-Unlimited
Subject Category: 07
Available electronically at http://www.sti.nasa.gov
This publication is available from the NASA Center for AeroSpace Information, 443-757-5802

13. SUPPLEMENTARY NOTES

14. ABSTRACT
Various new technologies currently under development may enable controlled blade shape variability, or so-called blade morphing, to be practically employed in aircraft engine fans and compressors in the foreseeable future. The current study is a relatively brief, preliminary computational fluid dynamics investigation aimed at partially demonstrating and quantifying the aerodynamic potential of fan rotor blade morphing. The investigation is intended to provide information useful for near-term planning, as well as aerodynamic solution data sets that can be subsequently analyzed using advanced acoustic diagnostic tools, for the purpose of making fan noise comparisons. Two existing fan system models serve as baselines for the investigation: the Advanced Ducted Propulsor fan with a design tip speed of 806 ft/sec and a pressure ratio of 1.294, and the Source Diagnostic Test fan with a design tip speed of 1215 ft/sec and a pressure ratio of 1.470. Both are 22-in. sub-scale, low-noise research fan/nacelle models that have undergone extensive experimental testing in the 9- by 15-foot Low Speed Wind Tunnel at the NASA Glenn Research Center. The study, restricted to fan rotor blade morphing only, involves a fairly simple blade morphing technique. Specifically, spanwise-linear variations in rotor blade-section setting angle are applied to alter the blade shape; that is, the blade is linearly retwisted from hub to tip. Aerodynamic performance comparisons are made between morphed-blade and corresponding baseline configurations on the basis of equal fan system thrust, where rotor rotational speed for the morphed-blade fan is varied to change the thrust level for that configuration. The results of the investigation confirm that rotor blade morphing could be a useful technology, with the potential to enable significant improvements in fan aerodynamic performance. Even though the study is very limited in scope and confined to simple geometric perturbations of two existing fan systems, the aerodynamic effectiveness of blade morphing is demonstrated by the configurations analyzed. In particular, for the Advanced Ducted Propulsor fan it is demonstrated that the performance levels of the original variable-pitch baseline design can be achieved using blade morphing instead of variable pitch, and for the Source Diagnostic Test fan the performance at important off-design operating points is substantially increased with blade morphing.

15. SUBJECT TERMS
Fan blades; Rotor blades; Torsion; Twisting; Angle of attach

16. SECURITY CLASSIFICATION OF:			17. LIMITATION OF ABSTRACT	18. NUMBER OF PAGES	19a. NAME OF RESPONSIBLE PERSON STI Help Desk (email:help@sti.nasa.gov)
a. REPORT U	b. ABSTRACT U	c. THIS PAGE U	UU	46	19b. TELEPHONE NUMBER *(include area code)* 443-757-5802